Spring 2010

Analysis of the theta-D filter as applied to hit-to-kill interceptors and satellite orbit determination

Michael W. Dancer

Department:

ANALYSIS OF THE THETA-D FILTER AS APPLIED TO HIT-TO-KILL INTERCEPTORS AND SATELLITE ORBIT DETERMINATION

by

MICHAEL WILLIAM DANCER

A THESIS

Presented to the Faculty of the Graduate School of the

MISSOURI UNIVERSITY OF SCIENCE AND TECHNOLOGY

In Partial Fulfillment of the Requirements for the Degree

MASTER OF SCIENCE IN AEROSPACE ENGINEERING

2010

Approved by

S. N. Balakrishnan, Co-Advisor
H. J. Pernicka, Co-Advisor
J. Sarangapani
J. Leitner

ABSTRACT

When designing feedback control systems, there is often a need for estimation methods that provide system information that is not readily available via sensors placed within the system. In many cases a sensor that measures a particular system state either does not exist or is prohibitively expensive. In addition, all realistic systems contain some degree of nonlinearity. This thesis focuses on two such cases: missile guidance with bearings-only measurements and GPS satellite orbit determination. In each case, a new nonlinear filter, the θ-D method, is used and evaluated for its performance in providing the necessary estimation.

To aid the filter in the bearings-only application, a guidance law is formulated that assists the filter in estimating the target location despite the lack of range measurement. An implementation procedure, called the Staggered Filter Concept, is also presented for implementing a continuous filter, such as the θ-D filter, with measurements taken at discrete intervals. This procedure is used to implement the orbit determination algorithm on the Missouri S&T Satellite Team M-SAT mission.

ACKNOWLEDGMENTS

I would first and foremost like to thank my advisors, Dr. Balakrishnan and Dr. Pernicka for their great support and advice throughout my academic career. I would also like to thank Dr Sarangapani and Dr. Leitner for serving on my graduate committee.

I am also greatly indebted to the entire M-SAT team for their continuing support and friendship. I would like to especially thank my colleagues at IST-Rolla, Jason Searcy and Nathan Harl, for their great camaraderie and of course ridicule for taking so long to finish this thing.

Lastly, but certainly not the least, I am forever gracious to my family. To my parents, who have been such a great source of inspiration and love, and to my brother and sister, who have provided endless encouragement throughout my collegiate days, I am incredibly thankful.

To anyone I may have missed, you have my apologies. I assure you, your support was greatly appreciated.

TABLE OF CONTENTS

LIST OF ILLUSTRATIONS

LIST OF TABLES

1. INTRODUCTION

1.1. MISSILE DEFENSE

In the aftermath of the Cold War and with technological advances, both in the United States and abroad, the need for an effective missile defense system is becoming more and more evident. Additionally, a near-miss is no longer sufficient, as hit-to-kill missiles are not equipped with proximity fuses as are typical Air Force missiles. The next generation of missile defense systems must be able to accurately track a large variety of highly maneuverable targets engaged in high range/high velocity intercept scenarios.

In order to ensure hit-to-kill accuracy in such a high energy engagement, advances in guidance, control, and estimation must be made, as any system is only as good as its weakest component. Guidance laws need to be developed that minimize miss distance despite large and highly random target evasive maneuvers, control systems need to be designed that are able to steer the missile with a high degree of precision, and estimation schemes need to be able to quickly and accurately estimate the system states that are to drive the guidance and control systems.

1.2. GUIDANCE AND CONTROL

The area of guidance and control is concerned with determining efficient methods for steering the missile to the intended target. The guidance portion generates acceleration commands which the autopilot controller enacts.

1.2.1. Guidance Laws. The guidance laws generate the required acceleration that must be produced by the missile in order to intercept the target. Several guidance laws exist that make use of the relative motion between the target and missile. Also, many guidance laws use, in one form or another, the acceleration of the target.

1.2.2. Autopilot Design. The purpose of the missile autopilot system is to use the missile actuators (fins, gyros, etc.) to supply the required acceleration. Care must be taken to ensure that the guidance law yields accelerations that the missile is capable of producing.

1.3. ESTIMATION

As mentioned in Section 1.2.1, the guidance law uses the relative position and velocity of the target, with respect to the missile, and also the target acceleration. In practicality, this information is not known entirely, therefore, an estimation scheme is required. Sensors built into the missile hardware measure certain quantities of the system such as range, angles, and various rates. The filter must then use this information, along with a dynamic model of the system, to produce the necessary information to be supplied to the guidance law.

1.3.1. Passive Measurements. When determining the relative distance between two objects, many sensors rely on a particular form of energy (laser, sound wave, etc.) that is reflected off of the target. This form of measurement is referred to as an active measurement system, as the detector must generate and emit energy, which could possibly be detected by the target. In many applications, including missile defense, it is desired that the measurement source be undetectable to the target. For this reason, research involving target intercept applications has shifted to using passive measurements only. Such measurements typically produce bearing angles only, although passive ranging is possible in some instances.

1.4. ORBIT DETERMINATION

In any space mission, the need for an accurate orbit determination method is required for satellite tracking. Accurate orbit determination is also necessary for accurate guidance in rendezvous and docking missions. The process of orbit determination has been studied and improved throughout the years, and multiple methods have been proposed. While the methods may vary, general orbit determination is achieved by application of a dynamic filter which processes some specified orbital measurements. This paper describes the orbit determination method planned for use on the Missouri University of Science and Technology's M-SAT mission.

1.4.1. M-SAT Mission. As per recommendation from NASA's Goddard Space Flight Center, the Missouri S&T Satellite design team at the Missouri University of Science and Technology is developing a pair of microsatellites that will demonstrate the capability of formation flight control by utilizing low-cost, off-the-shelf technologies. This mission will consist of a pair of satellites that separate on orbit and establish a desired formation of 50 meters in track. During the formation flight phase the onboard propulsion system will be used to maintain the desired 50 meter separation. The satellite pair is depicted in Figure 1.1 below in their mated launch configuration.

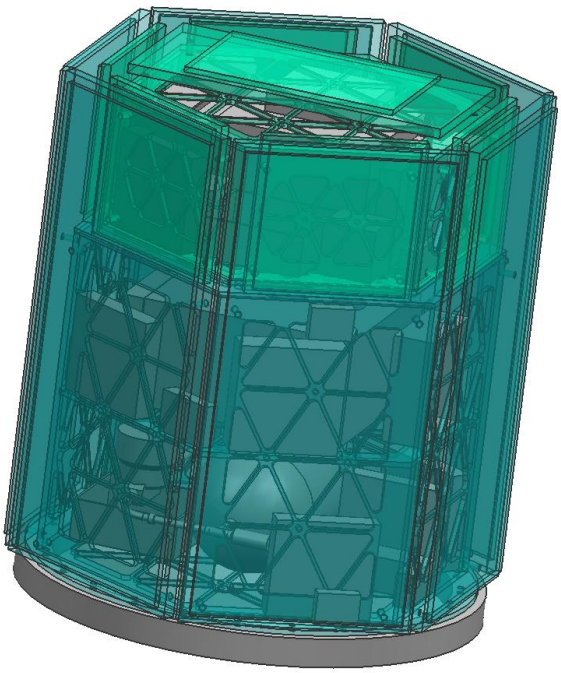

Figure 1.1. M-SAT Microsatellites

The larger of the two satellites, Missouri Rolla Satellite, or MR SAT, will be equipped with a cold-gas propulsion system and serve as the follower in the formation flight phase. The smaller of the two, Missouri Rolla Second Satellite, or MRS SAT, will

serve as the leader spacecraft. MR SAT will also be the primary means of communication with the satellites by ground controllers as it is the only of the pair with space to ground communication ability.

Since the entire M-SAT mission is being developed as a demonstration flight, a newly developed orbit determination technique has been selected for onboard orbit navigation. The satellites will be demonstrating the efficacy of a new nonlinear filter developed at Missouri S&T, the θ-D filter, which will be used to process GPS data for determining the satellites' orbit. The nonlinear θ-D filter will be implemented using a new concept, referred to as the staggered filter, which allows continuous filters to be implemented in a discrete time sense.

2. REVIEW OF LITERATURE

2.1. CONTROL OR AUTOPILOT DESIGN

A large portion of papers on missile guidance and control have focused on the area of missile control or autopilot design, see Refs. 1, 6, 7, 11, 19, 24, 38, 46, 49, 54, and 56. Theoretical bases for these papers include optimal control, feedback linearization, state dependent Riccati equations (SDRE), and θ-D. There have also been several papers published recently using the concept of sliding mode in the area of control, guidance and estimation, see Refs. 15, 23, 28, 34, 39-41, and 47.

2.2. GUIDANCE LAW DESIGN

The majority of guidance laws are formulated on the relative kinematics between the target and the missile [30, 58]. Many guidance laws that have been formulated are based on variations of the concept of proportional navigation, in which a constant target velocity is assumed, see Refs. 2, 8, 10, and 12. In 2003, Savkin et al. developed a modified H_∞ control based guidance law that was shown to provide much better performance, in the sense of disturbance rejection, than the linear quadratic regulator (LQR) based optimal guidance law. The H_∞ guidance law also has an output feedback structure that is more realistic than the LQR method, which assumes that all states are available. Later in 2003, Raju and Ghose proposed a novel midcourse guidance law based on an empirical virtual sliding target (VST) approach. This law uses the conventional proportional navigation (ProNav) guidance law while exploiting the aerodynamic characteristics of the missile's flight through the atmosphere. The trajectory of the missile is controlled via the speed of a virtual target, which slides towards a predicted intercept point (PIP) during the midcourse phase.

Lyapunov theory has also been used to improve conventional guidance schemes [43]. Recently, Yanushevsky and Boord improved the conventional ProNav guidance law by using Lyapunov theory. In Reference 57, the guidance problem was formulated as a stability problem and a Lyapunov function was chosen as the square of the line-of-sight (LOS) derivative. Also, Lechevin and Rabbath have used a new set of state space

variables in the missile guidance problem which led to an easier Lyapunov-based synthesis, where trigonometric functions of the LOS and LOS derivative were used, see Reference 20. This approach provides uniform, ultimate boundedness of the missile-target system for the case of highly maneuvering targets. Similar to the area of control, many recent papers have used the sliding mode technique for the derivation of guidance laws, see Refs. 28, 34, 37, and 41.

Game theory has also made its contributions to the development of guidance laws for the target-intercept problem [1]. Ben-Asher and Levinson used a "trajectory shaping" term, which was added to the cost function by augmenting it with a quadratic-integral term of the state variables, see Reference 5. It was shown that the trajectory shaping terms led to attenuation of the disturbance that is created by a random maneuvering target.

2.3. ESTIMATION

The concept of estimation and observers plays a crucial role in the target-intercept problem, for guidance laws are only as effective as the accuracy of the estimated states that are used in calculating the command acceleration, see Refs. 3, 4, 14, 17, 25, 37, 42, 44, and 52. Oshman and Arad investigated a new method to reduce the estimation delay in the target acceleration estimation problem. The idea is based on the correlation existing between the target's orientation, measured using an imaging sensor, and its evasive maneuvers. Three estimators, including two extended Kalman filters (EKFs) and an interacting multiple model filter, were designed and used to demonstrate the performance improvement, see Reference 31.

2.4. INTEGRATED GUIDANCE AND CONTROL

In recent years, the missile-intercept problem has turned towards the concept of integrated guidance and control (IGC), in which the guidance and control problems were solved in a single architecture to promote synergy between the system components.

Lin and Yueh were the first to address the use of an IGC design in the missile-intercept problem [24]. An optimal controller was designed, which combined the guidance law and autopilot design into a single framework, to minimize a quadratic cost functional subject to the system dynamics. The advantages gained in this optimal control law were minimization of, in the presence of unmodeled errors, the root mean square (RMS) miss distance, the terminal angle of attack, the pitch rate, and the control surface "flapping" rate. However, these papers only dealt with non-maneuvering targets. Evers et al. extended the concepts presented in Reference 24 to include a target acceleration model as a first order Markov process. The resulting IGC law was expected to be less sensitive to the errors in estimating the current target acceleration, see Reference 16.

Another IGC design was proposed by Menon and Ohlmeyer. This design combined the feedback linearization method with the Linear Quadratic Regulator (LQR) technique to design a nonlinear integrated guidance and control law for homing missiles. The IGC design was presented in three formulations, which were based upon three different guidance objectives, then a 6DOF nonlinear dynamic model of an air-to-air homing missile was simulated. Each of three IGC schemes achieved a specific favorable performance over the other, see Reference 27. The disadvantages of feedback linearization are as follows: beneficial nonlinearities may be completely removed and result in a large control and feedback linearization is only applicable to systems which are feedback linearizable.

The IGC concept was further extended by employing the State Dependent Riccati Equation (SDRE) technique [9] to deal with a nonlinear model and 3-D motion. The problem was cast as an infinite-horizon type problem, and a command generator was used to prevent actuator saturation and also to meet a terminal aspect angle constraint. The design was evaluated using a 6DOF nonlinear missile model with two types of target models: non-maneuvering targets and weaving targets. The numerical results demonstrated the feasibility of designing IGC systems for the next generation high-performance missile systems, see Reference 26. Palumbo et al. at the Johns Hopkins Applied Physics Laboratory (publication restricted) have been working on IGC schemes using finite time SDRE based schemes [32].

The downside to the SDRE approach to IGC design is that solving the state dependent Riccati equation on-line is very time-consuming, especially for a 6DOF missile with an integrated guidance design. As the system order grows the SDRE approach requires significant computational capability, for on-line implementation, that is sometimes not feasible. Xin and Balakrishnan successfully applied the θ-D method to the IGC design based on the same nonlinear missile model and achieved some good preliminary results. The θ-D method is a sub-optimal control scheme that approximates the solution to the SDRE and applies disturbance terms to the SDRE in order to prevent large control inputs. Compared to the SDRE approach, the θ-D controller gives a closed-form solution and is easy to implement, see Reference 55.

2.5. ORBIT DETERMINATION

Early orbit determination methods relied on observational data obtained from ground-based telescopes. Before dynamic filters were known, the data were processed by solving relatively complicated orbital equations of motion. A popular method was developed by Gauss and used angle measurements only [48]. This method was successfully used, by Gauss, to predict the return of Ceres in 1801. Over the years, the methods for obtaining the telescopic data have been refined, however the general processing methods have remained the same.

With the introduction of dynamic filter concepts and accurate numerical integration schemes, more orbit determination options became available. The most common method is to use the Global Positioning System (GPS) to obtain, through triangulation, the position of the GPS receiver. The GPS uses a network of orbiting satellites which continually send radio signals to receivers with a direct line-of-sight. The time required for the signal to reach the receiver is used to determine the range to the receiver, and with four available measurements, it is possible to determine the position of the receiver. This system has been used successfully on several satellite missions [21, 22, 33].

Another method of orbit determination that has been used successfully is to measure the Earth's magnetic field [13]. This particular method can be used not only for orbit determination, but also the determination of the satellite attitude. This process was incorporated in the Magnetometer Navigation (MAGNAV) Inflight Experiment [45].

3. θ-D FILTER FORMULATION

3.1. CONTROL/FILTER PARALLELISM

The concept of control is to use inputs, e.g. forces, torques, etc., to a system to change the behavior of the system in a desirable manner. This is most readily accomplished through feedback control where the system inputs are calculated based upon the current state of the system. Consider the general dynamic system of the form

$$\dot{x} = f\left(x,u\right) + \Delta_x \tag{1}$$

where f is the dynamic model of the system, x is the system state vector, u is the system input vector, and Δ_x is a disturbance term that accounts for unmodeled dynamics and system uncertainties.

Typically, the control problem is transformed into a regulator type problem where it is desired that $x \to 0$ as time progresses towards infinity. For tracking problems, x would represent system tracking errors. The control problem then becomes a matter of trying to find a suitable function, the control law, of the form

$$u = g\left(x\right) \tag{2}$$

which causes $x \to 0$ in the presence of disturbances.

The problem encountered with feedback control is that complete knowledge of all system states is required for calculation of the input control. The objective of a filter is to produce estimates for the system states by using a series of sensor measurements to effectively "control" the state of a fictitious dynamic system, $\hat{x}$, so that $\hat{x} \to x$ as time progresses towards infinity. The measurements are given by

$$y = h\left(x\right) + v \tag{3}$$

where v is noise that affects the sensor measurements.

Generally, the filter model is taken as the system model it is supposed to estimate plus an extra term to incorporate the measurement control.

$$\dot{\hat{x}} = f\left(\hat{x}, u\right) + k\left(y, \hat{x}\right) \tag{4}$$

By taking the difference between the estimated and actual states, the filter error dynamics are obtained as

$$\dot{e} = f\left(e, u\right) + k\left(y, \hat{x}\right) + \Delta_e \tag{5}$$

where Δ_e is a disturbance term that accounts for modeling errors, system uncertainties, as well as errors incurred through system nonlinearities and measurement noise.

In a parallel fashion to the regulator control problem, the filter problem has now become a matter of finding a suitable function, k, that causes $e \to 0$ in the presence of the disturbances. Because of this parallelism, many of the techniques developed for system control can also be used for the filter application as well.

3.2. STATE DEPENDANT RICATTI EQUATION FILTER (SDREF)

The State Dependant Riccati Equation Filter (SDREF) makes use of the parallelism between control and filter problems. The State Dependant Riccati Equation (SDRE) controller and its filter counterpart, SDREF, are described in the following subsections.

3.2.1. Linear Systems. The SDRE controller is an extension of the optimal Linear Quadratic Regulator (LQR) controller to nonlinear systems. Consider the linear system described by

$$\dot{x} = Ax + Bu \tag{6}$$

Additionally, a quadratic cost function is defined as

$$J = \int_0^\infty \left(x^T Q x + u^T R u \right) dt \tag{7}$$

The LQR controller minimizes the cost function, *J*, with the control law

$$u = -R^{-1} B^T S x \tag{8}$$

where *S* is the solution to the nonlinear Algebraic Riccati Equation (ARE)

$$0 = Q + SA + A^T S - SBR^{-1} B^T S \tag{9}$$

In a parallel manner, an optimal observer, the Kalman filter, is obtained from

$$\dot{\hat{x}} = A\hat{x} + Bu + SH^T W^{-1} \left(y - H\hat{x} \right) \tag{10}$$

where the measurements are given from $y = Hx + w$, *W* is the power spectral density of the random noise, *w*, and *S* is the solution to the ARE

$$0 = V + AS + SA^T - SH^T W^{-1} HS \tag{11}$$

where *V* is the power spectral density for the system disturbances, Δ_x, referred to as process noise.

3.2.2. Nonlinear Systems. To extend the LQR controller to nonlinear systems, the nonlinear system is first cast into a linear-like structure.

$$\dot{x} = F\left(x\right) x + G\left(x\right) u \tag{12}$$

Just as was done for the linear system, the control law that minimizes the cost function, *J*, is given by

$$u = -R^{-1}G^T(x)S(x)x$$

where *S* is the state-dependant solution to the State Dependant Riccati Equation (SDRE)

$$0 = Q + S(x)F(x) + F^T(x)S(x) - S(x)G(x)R^{-1}G^T(x)S(x) \tag{13}$$

Unlike the LQR controller, the SDRE controller requires that the SDRE be solved online at each time step since the coefficient matrices are continually changing as the system state changes.

Using the parallelism between controllers and filters, the SDREF is obtained from

$$\dot{\hat{x}} = F(\hat{x})\hat{x} + G(\hat{x})u + S(\hat{x})H(\hat{x})^T W^{-1}\left[y - H(\hat{x})\hat{x}\right] \tag{14}$$

where the measurements are cast in the linear-like structure, $y = H(x)x + w$, and *S* is the solution to the SDRE

$$0 = V + F(\hat{x})S(\hat{x}) + S(\hat{x})F^T(\hat{x}) - S(\hat{x})H^T(\hat{x})W^{-1}H(\hat{x})S(\hat{x}) \tag{15}$$

which must be solved continually online.

3.3. θ APPROXIMATION METHOD

The problem with the SDREF is that the Riccati equation must be solved in real time, and this task requires a significant amount of computation time. One method

proposed for solving the Riccati equation is known as the θ approximation method. This method works by assuming the solution to the Riccati equation as a power series in θ.

$$S(\hat{x}) = \sum_{i=0}^{\infty} T_i(\hat{x}, \theta)\theta^i \tag{16}$$

Next, the dynamic coefficient matrices are factored into constant and state dependent terms.

$$F(\hat{x}) = A_0 + \frac{A(\hat{x})}{\theta}\theta \tag{17}$$

$$H(\hat{x}) = C_0 + \frac{C(\hat{x})}{\theta}\theta \tag{18}$$

By substituting Equations 16-18 into the Riccati equation and matching coefficients of θ^i, the following recursive equations are found.

$$0 = V + A_0T_0 + T_0A_0^T - T_0C_0^TW^{-1}C_0T_0 \tag{19.0}$$

$$\begin{aligned} &T_1\left(A_0 - T_0C_0^TW^{-1}C_0\right)^T + \left(A_0 - T_0C_0^TW^{-1}C_0\right)T_1 \\ &= -\frac{T_0\left(A(\hat{x}) - T_0C_0^TW^{-1}C(\hat{x})\right)^T}{\theta} - \frac{\left(A(\hat{x}) - T_0C_0^TW^{-1}C(\hat{x})\right)T_0}{\theta} \end{aligned} \tag{19.1}$$

$$\begin{aligned} &T_2\left(A_0 - T_0C_0^TW^{-1}C_0\right)^T + \left(A_0 - T_0C_0^TW^{-1}C_0\right)T_2 \\ &= -\frac{T_1\left(A(\hat{x}) - T_0C_0^TW^{-1}C(\hat{x})\right)^T}{\theta} - \frac{\left(A(\hat{x}) - T_0C_0^TW^{-1}C(\hat{x})\right)T_1}{\theta} \\ &+\left(C_0T_1 + \frac{C(\hat{x})}{\theta}T_0\right)^T W^{-1}\left(C_0T_1 + \frac{C(\hat{x})}{\theta}T_0\right) \end{aligned} \tag{19.2}$$

$$\vdots \qquad \vdots$$

$$
\begin{aligned}
&T_n\left(A_0 - T_0 C_0{}^T W^{-1} C_0\right)^T + \left(A_0 - T_0 C_0{}^T W^{-1} C_0\right) T_n \\
&= -\frac{T_{n-1}\left(A(\hat{x}) - T_0 C_0{}^T W^{-1} C(\hat{x})\right)^T}{\theta} - \frac{\left(A(\hat{x}) - T_0 C_0{}^T W^{-1} C(\hat{x})\right) T_{n-1}}{\theta} \\
&+ \sum_{j=1}^{n-1} \left(C_0 T_j + \frac{C(\hat{x})}{\theta} T_{j-1} \right)^T W^{-1} \left(C_0 T_{n-j} + \frac{C(\hat{x})}{\theta} T_{n-j-1} \right)
\end{aligned}
\qquad (19.n)
$$

Equation 19.0 can be seen to be another Riccati equation, but unlike the SDRE is state independent and therefore need only be solved once offline. Equations 19.1-*n* are linear Lyapunov equations which require significantly less computation time to solve. Once Equations 19.0-*n* are solved, the solution to the SDRE is simply found from Equation 16. Since Equation 16 must be truncated at some point, this method produces only an approximate solution to the SDRE, but this approximate solution is obtained much more easily in real time.

3.4. DISTURBANCE TERMS

The θ approximation method does have its downfalls. Consider a system in which $A(x) = x^2$. If the initial system state, x_0, is large, $A(x)$ will also be large and will produce recursively larger T_i matrices. This could pose numerical issues during the filter operation. Additionally, the θ approximation method does not have guaranteed convergence. To remedy these issues, a sub-optimal filter is proposed that solves a modified version of the Riccati equation. This new filter will be referred to as the θ-D filter herein.

The θ-D filter adds a series of disturbance terms to The Riccati equation and solves the disturbed Riccati equation

$$
0 = \left[V + \sum_{j=1}^{\infty} D_j(\hat{x}, \theta) \theta^j \right] + F(\hat{x}) S(\hat{x}) + S(\hat{x}) F^T(\hat{x}) - S(\hat{x}) H^T(\hat{x}) W^{-1} H(\hat{x}) S(\hat{x}) \quad (20)
$$

where the disturbance terms, $D_j(\hat{x},\theta)$, are design parameters and are chosen such that

$$\left\| \sum_{j=1}^{\infty} D_j(\hat{x},\theta)\theta^j \right\| \ll \|V\| \tag{21}$$

This condition ensures that the solution to the disturbed Riccati equation will closely approximate the solution to the SDRE. Application of the θ approximation method to the disturbed Riccati equation results in the following recursion equations.

$$0 = V + A_0 T_0 + T_0 A_0^T - T_0 C_0^T W^{-1} C_0 T_0 \tag{22.0}$$

$$\begin{aligned} &T_1\left(A_0 - T_0 C_0^T W^{-1} C_0\right)^T + \left(A_0 - T_0 C_0^T W^{-1} C_0\right) T_1 \\ &= -\frac{T_0\left(A(\hat{x}) - T_0 C_0^T W^{-1} C(\hat{x})\right)^T}{\theta} - \frac{\left(A(\hat{x}) - T_0 C_0^T W^{-1} C(\hat{x})\right) T_0}{\theta} - D_1 \end{aligned} \tag{22.1}$$

$$\begin{aligned} &T_2\left(A_0 - T_0 C_0^T W^{-1} C_0\right)^T + \left(A_0 - T_0 C_0^T W^{-1} C_0\right) T_2 \\ &= -\frac{T_1\left(A(\hat{x}) - T_0 C_0^T W^{-1} C(\hat{x})\right)^T}{\theta} - \frac{\left(A(\hat{x}) - T_0 C_0^T W^{-1} C(\hat{x})\right) T_1}{\theta} \\ &+ \left(C_0 T_1 + \frac{C(\hat{x})}{\theta} T_0\right)^T W^{-1} \left(C_0 T_1 + \frac{C(\hat{x})}{\theta} T_0\right) - D_2 \end{aligned} \tag{22.2}$$

$$\vdots \qquad\qquad \vdots$$

$$\begin{aligned} &T_n\left(A_0 - T_0 C_0^T W^{-1} C_0\right)^T + \left(A_0 - T_0 C_0^T W^{-1} C_0\right) T_n \\ &= -\frac{T_{n-1}\left(A(\hat{x}) - T_0 C_0^T W^{-1} C(\hat{x})\right)^T}{\theta} - \frac{\left(A(\hat{x}) - T_0 C_0^T W^{-1} C(\hat{x})\right) T_{n-1}}{\theta} \\ &+ \sum_{j=1}^{n-1} \left(C_0 T_j + \frac{C(\hat{x})}{\theta} T_{j-1}\right)^T W^{-1} \left(C_0 T_{n-j} + \frac{C(\hat{x})}{\theta} T_{n-j-1}\right) - D_n \end{aligned} \tag{22.n}$$

The disturbance terms can now be chosen so as to alleviate the problem of large initial observer gains. These matrices are chosen as

$$D_j\left(\hat{x},\theta\right)=k_j e^{-l_j t}\left(-\frac{T_{j-1}A^T\left(\hat{x}\right)}{\theta}-\frac{A\left(\hat{x}\right)T_{j-1}}{\theta}\right) \tag{23}$$

where each $k_j > 0$ determines the canceling effect of the disturbance and the $l_j > 0$ term allows the disturbance to die off as time progresses. With the disturbance terms defined, Equations 22.0-*n* are solved, and Equation 16 then produces an appoximate solution to the SDRE.

3.4.1. Proof of Convergence. It can also be shown that proper selection of the constants, k_j and l_j, will also guarantee convergence of Equation 16. This proof is provided in Appendix A.

3.5. SUMMARY

This subsection provides a summary of the implementation procedure for the θ-D filter technique.

The first step is to cast the system model and measurement function into a linear-like structure. Furthermore, the state dependant coefficient matrices need to be factored into a constant and state dependant term. This procedure is easily accomplished by setting $A_0 = F(x_0)$ and $C_0 = H(x_0)$, then $A(x)$ and $C(x)$ are simply the remainders. At this point it is convenient to select the k_j and l_j parameters. From experience in using the θ-D filter on various problems, the first three terms in Equation 16 are usually sufficient to produce the desired approximate solution to the SDRE.

Next, Equation 22.0 is solved for T_0. This only needs to be performed once! Also, it is convenient to calculate and store the matrix $K_0 = A_0 - T_0 C_0^T W^{-1} C_0$ for later use. Then, at each time step, the matrices, T_i for $i = 1,2,\ldots$, are recursively calculated from

$$T_n K_0^T + K_0 T_n = -\frac{T_{n-1}K^T}{\theta}-\frac{KT_{n-1}}{\theta}+P-D_n \tag{24}$$

where the disturbance terms are calculated from Equation 23, $K = A(x) - T_0 C_0{}^T W^{-1} C(x)$, and

$$P = \sum_{j=1}^{n-1} \left(C_0 T_j + \frac{C(\hat{x})}{\theta} T_{j-1} \right)^T W^{-1} \left(C_0 T_{n-j} + \frac{C(\hat{x})}{\theta} T_{n-j-1} \right) \tag{25}$$

Again, experience with θ-D indicates that calculation up to T_2 is typically sufficient. Also, it should be noted that the variable θ is simply a means to produce a power series solution for the SDRE, and the solution turns out to be independent of the choice of θ, therefore $\theta = 1$ is generally used.

Finally, the solution to the SDRE is obtained from Equation 16 and the filter dynamic model is given by Equation 14.

4. EQUATIONS OF MOTION

4.1. MISSILE ENGAGEMENT

This section presents the dynamic equations of motion (EOMs) used in the missile intercept problem.

4.1.1. 2-D Scenario. The 2-D missile engagement is depicted in Figure 4.1 below. The states for the system are r, the relative range, and θ, the bearing angle measured from the initial line-of-sight (LOS), r_0, to the current LOS.

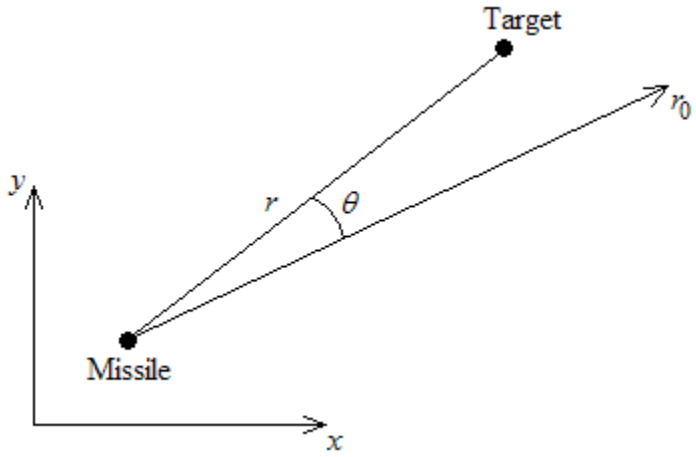

Figure 4.1. 2-D Missile Engagement

Using polar coordinates, the EOMs for the 2-D scenario are

$$\ddot{r} = r\dot{\theta}^2 + a_{t_r} - a_{m_r} \tag{26}$$

$$r\ddot{\theta} = -2\dot{r}\dot{\theta} + a_{t_\theta} - a_{m_\theta} \tag{27}$$

where a_t and a_m are the target and missile accelerations, respectively, with the r and θ subscripts indicating the radial and tangential components, respectively. Since passive measurements are used, the system measurement is $y = \theta + w$.

4.1.2. 3-D Scenario. The 3-D missile engagement is depicted in Figure 4.2 below. The states for the system are r, the relative range, θ, the bearing angle measuring the azimuth, and ϕ, the bearing angle measuring the elevation. The two bearing angles are measured from the initial LOS to the current LOS.

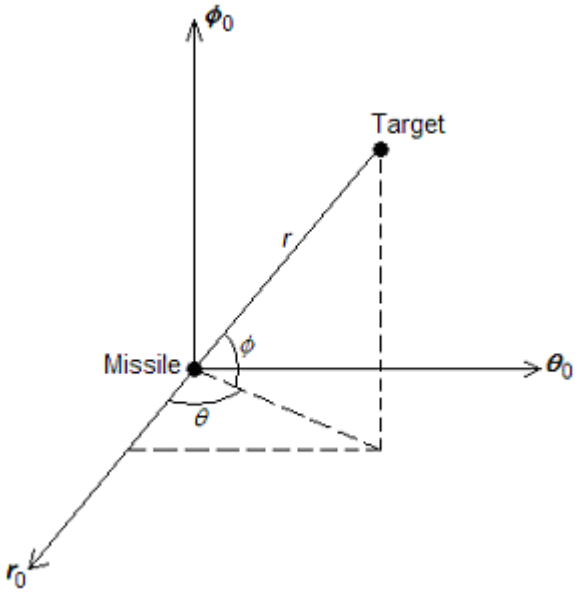

Figure 4.2. 3-D Missile Engagement

Using spherical coordinates, the EOMs for the 3-D scenario are

$$\ddot{r} = r\left(\dot{\theta}^2 \cos^2\phi + \dot{\phi}^2\right) + a_{t_r} - a_{m_r} \tag{28}$$

$$r\ddot{\theta}\cos\phi = -2\dot{r}\dot{\theta}\cos\phi + 2r\dot{\theta}\dot{\phi}\sin\phi + a_{t_\theta} - a_{m_\theta} \tag{29}$$

$$r\ddot{\phi} = -r\dot{\theta}^2 \sin\phi\cos\phi - 2\dot{r}\dot{\phi} + a_{t_\phi} - a_{m_\phi} \tag{30}$$

where a_t and a_m are the target and missile accelerations, respectively, with the r, θ, and ϕ subscripts indicating the radial, azimuth, and elevation components, respectively. Since passive measurements are used, the system measurements are $y = [\theta\ \phi]^T + w$.

4.2. TARGET ACCELERATION MODELING

For the results presented in Section 7, the filter modeled the target acceleration as a first order Markov process. This is to say

$$\dot{a}_{t_r} = -\lambda_r a_{t_r} + \nu_r \tag{31}$$

$$\dot{a}_{t_\theta} = -\lambda_\theta a_{t_\theta} + \nu_\theta \tag{32}$$

$$\dot{a}_{t_\phi} = -\lambda_\phi a_{t_\phi} + \nu_\phi \tag{33}$$

where ν_r, ν_θ, and ν_ϕ are random processes that account for the random nature of target evasive maneuvers.

4.3. MISSILE ACTUATOR MODELING

In any mechanical system, there is always a lag between commanded input and the actual input delivered to the system. This lag is a result of the finite time it takes for control actuators to transition from one commanded input to another. For the results presented in Section 7, the missile actuator lag is modeled as first order lag. This is to say

$$\dot{u} = -\lambda_u \left(u - u_c\right) \tag{34}$$

where u is the actual input to the system and u_c is the commanded input. For the missile intercept problem studied in this thesis, u is the missile acceleration, a_m, and u_c is the acceleration obtained from the guidance law.

4.4. LINEAR-LIKE STRUCTURE

This subsection presents the EOMs, found in Section 4.1, cast in a linear-like structure required for use of the θ-D filter. There are many ways of factoring the system EOMs into a linear-like structure, but since the θ-D technique approximately solves the SDRE, the state dependent matrices must be locally detectable. The factorization presented in this subsection is not unique, but does demonstrate sufficient performance when used in the θ-D filter.

4.4.1. 2-D. There are two degrees of freedom in the 2-D scenario and, with the target acceleration, the system has six separate states. The state vector for the 2-D scenario is chosen to be $x = \begin{bmatrix} r & \theta & \dot{r} & \dot{\theta} & a_{t_r} & a_{t_\theta} \end{bmatrix}^T$. With the state as selected, $F(x)$ and $G(x)$ are chosen to be

$$F(x) = \begin{bmatrix} 0 & 0 & 1 & 0 & 0 & 0 \\ 0 & 0 & 0 & 1 & 0 & 0 \\ x_4^{\,2} & 0 & 0 & 0 & 1 & 0 \\ 0 & 0 & 0 & -2x_3/x_1 & 0 & 1/x_1 \\ 0 & 0 & 0 & 0 & -\lambda_r & 0 \\ 0 & 0 & 0 & 0 & 0 & -\lambda_\theta \end{bmatrix} \tag{35}$$

$$G(x) = \begin{bmatrix} 0 & 0 & -1 & 0 & 0 & 0 \\ 0 & 0 & 0 & -1/x_1 & 0 & 0 \end{bmatrix}^T \tag{36}$$

The $x_4^{\,2}$ term in the first column of F is important for ensuring local detectability in the system. This is demonstrated in Section 5, which describes the formulation of the Observability Enhanced Guidance Law (OEGL).

In the 2-D scenario with passive measurements, the only measurement is the bearing angle, θ. Since polar coordinates were used in developing the EOMs, the measurement function is already linear with $H(x)$ given by

$$H(x) = \begin{bmatrix} 0 & 1 & 0 & 0 & 0 & 0 \end{bmatrix} \tag{37}$$

4.4.2. 3-D. There are three degrees of freedom in the 3-D scenario and, with the target acceleration, the system has nine separate states. The state vector for the 3-D scenario is chosen to be $x = \begin{bmatrix} r & \theta & \phi & \dot{r} & \dot{\theta} & \dot{\phi} & a_{t_r} & a_{t_\theta} & a_{t_\phi} \end{bmatrix}^T$. With the state as selected, $F(x)$ and $G(x)$ are chosen to be

$$F(x) = \begin{bmatrix} 0 & I & 0 \\ F_{21}(x) & F_{22}(x) & F_{23}(x) \\ 0 & 0 & -\lambda \end{bmatrix} \tag{38}$$

$$G(x) = \begin{bmatrix} 0 & 0 & -1 & 0 & 0 & 0 \\ 0 & 0 & 0 & -1/x_1 & 0 & 0 \end{bmatrix}^T \tag{39}$$

where

$$F_{21}(x) = \begin{bmatrix} x_5^{\,2}\cos^2 x_3 + x_6^{\,2} & 0 & 0 \\ 0 & 0 & 0 \\ 0 & 0 & 0 \end{bmatrix} \tag{40}$$

$$F_{22}(x) = \begin{bmatrix} 0 & 0 & 0 \\ -2x_5/x_1 & 0 & 2x_5 \tan x_3 \\ -2x_6/x_1 & -x_5 \sin x_3 \cos x_3 & 0 \end{bmatrix} \tag{41}$$

$$F_{23}(x) = \begin{bmatrix} 1 & 0 & 0 \\ 0 & 1/x_1 \cos x_3 & 0 \\ 0 & 0 & 1/x_1 \end{bmatrix} \tag{42}$$

$\lambda = diag([\lambda_r \ \lambda_\theta \ \lambda_\phi])$, and I is the 3x3 identity matrix.

The $x_5^2\cos^2 x_3 + x_6^2$ term in the first column of F_{21} is important for ensuring local detectability in the system. This is demonstrated in Section 5, which describes the formulation of the Observability Enhanced Guidance Law (OEGL).

In the 3-D scenario with passive measurements, the only measurements are the bearing angles, θ and ϕ. Since spherical coordinates were used in developing the EOMs, the measurement function is already linear with $H(x)$ given by

$$H(x) = \begin{bmatrix} 0 & 1 & 0 & 0 & 0 & 0 & 0 & 0 & 0 \\ 0 & 0 & 1 & 0 & 0 & 0 & 0 & 0 & 0 \end{bmatrix} \tag{43}$$

4.5. LOW EARTH ORBIT MODEL

In this section the dynamic model used by the θ-D filter for orbit determination is developed. The model incorporates Earth's gravity field, with the perturbation due to the Earth's equatorial bulge, gravitational effects due to the Sun and the Moon, and atmospheric drag. The acceleration for each perturbation is formulated, and the combined accelerations produce the desired dynamic model. In the sections that follow, $\boldsymbol{r}$ and $\boldsymbol{v}$ are the satellite position and velocity, respectively, and r represents the satellite orbital radius.

4.5.1. Earth's gravitational field. The Earth's gravitational field is modeled to incorporate the two dominant effects: spherical and non-spherical. The spherical effect results by assuming a spherically symmetric Earth and the dominant non-spherical effect results from the Earth's equatorial bulge.

4.5.1.1 Spherical effect. With μ_E representing the Earth's gravitational parameter, the acceleration due to a spherical Earth is [48]

$$\boldsymbol{a}_{geo} = -\frac{\mu_E}{r^3}\boldsymbol{r} \tag{44}$$

4.5.1.2 Non-spherical effect. The Earth, however, is not spherically symmetric, and the most dominant non-spherical effect occurs as a result of the equatorial bulge. This effect is best modeled via the second zonal harmonic which produces an additional gravitational potential given as [48]

$$U_2 = -\frac{1}{2}J_2\frac{\mu_E}{r}\left(\frac{r_E}{r}\right)^2\left(3\sin^2\phi - 1\right) \tag{45}$$

where r_E is the mean equatorial radius of the Earth, ϕ is the satellite latitude, and J_2 is the second zonal harmonic coefficient. The perturbative acceleration is found from the gradient of U_2. Using spherical coordinates the gradient is

$$\boldsymbol{a}_{J2} = \nabla U_2 = \frac{3}{2}J_2\frac{\mu_E}{r^2}\left(\frac{r_E}{r}\right)^2\left(3\sin^2\phi - 1\right)\boldsymbol{u}^1 - 3J_2\frac{\mu_E}{r}\left(\frac{r_E}{r}\right)^2\sin\phi\cos\phi\,\boldsymbol{u}^2 \tag{46}$$

where $\boldsymbol{u}^1$ and $\boldsymbol{u}^2$ are the 1st and 2nd contravariant basis vectors, respectively, in the spherical coordinate system. In this system $\boldsymbol{u}^1 = \boldsymbol{r}/r$ and $\boldsymbol{u}^2 = -\sin\phi\cos\theta\boldsymbol{i} - \sin\phi\sin\theta\boldsymbol{j} + \cos\phi\boldsymbol{k} = [-xz\boldsymbol{i} - yz\boldsymbol{j} + (x^2+y^2)\boldsymbol{k}]/r^2\cos\phi$. The basis vector $\boldsymbol{u}^2$ can be represented in matrix form as $\boldsymbol{u}^2 = R_\phi\boldsymbol{r}/r^2\cos\phi$ where

$$R_\phi = \begin{bmatrix} -z & 0 & 0 \\ 0 & -z & 0 \\ x & y & 0 \end{bmatrix} \tag{47}$$

With the basis vector in this form, the perturbative acceleration due to Earth's equatorial bulge is

$$\boldsymbol{a}_{J2} = -\frac{\mu_E}{r^3}\left[-\frac{3}{2}J_2\left(\frac{r_E}{r}\right)^2\left(3\sin^2\phi - 1\right)I + 3\frac{J_2}{r}\left(\frac{r_E}{r}\right)^2 \sin\phi R_\phi\right]\boldsymbol{r} \tag{48}$$

4.5.2. Third Body Effects. The dominant third body perturbations acting on a satellite in low Earth orbit are from the Sun and the Moon.

4.5.2.1 Sun. The perturbation due to the Sun as a third body is modeled as [48]

$$\boldsymbol{a}_{sun} = \mu_S\left(\frac{\boldsymbol{r}_{se}}{r_{se}^{\,3}} - \frac{\boldsymbol{r}_{st}}{r_{st}^{\,3}}\right) \tag{49}$$

where $\boldsymbol{r}_{st}$ and $\boldsymbol{r}_{se}$ are vectors from the Sun to the satellite and the Sun to the Earth, respectively, and r_{st} and r_{se} are the magnitudes of $\boldsymbol{r}_{st}$ and $\boldsymbol{r}_{se}$, respectively. Assuming that the satellite is in low Earth orbit, so that $r_{st} \approx r_{se} \approx d_S$, the mean distance between the Earth and the Sun, and by noting that $\boldsymbol{r}_{st} - \boldsymbol{r}_{se} = \boldsymbol{r}$, the perturbation due to the Sun's gravity field can be approximated as

$$\boldsymbol{a}_{sun} \approx -\frac{\mu_S}{d_S^{\,3}}\boldsymbol{r} \tag{50}$$

4.5.2.2 Moon. Following a similar procedure as was done for the Sun's gravitational field, the perturbation due to the Moon's gravity field can be approximated as

$$\boldsymbol{a}_{moon} \approx -\frac{\mu_M}{d_M{}^3}\boldsymbol{r} \tag{51}$$

where d_M is the mean distance between the Earth and the Moon.

4.5.3. Atmospheric Drag. The force due to atmospheric drag has a magnitude of qSc_D where q is the dynamic pressure, $q = \rho V_{rel}^2/2$ where ρ is the atmospheric density and V_{rel} is the satellite velocity magnitude relative to the atmosphere, S is the reference area, and c_D is the satellite drag coefficient. The drag force acts in the opposite direction as the satellite velocity vector relative to the atmosphere, $\boldsymbol{V}_{rel}$. By defining the ballistic drag coefficient as $\beta = m/Sc_D$, with m being the satellite mass, the acceleration due to atmospheric drag is

$$\boldsymbol{a}_{drag} = -\frac{\rho}{2\beta}V_{rel}\boldsymbol{V}_{rel} \tag{52}$$

To model the atmosphere, assume an exponential density decay, $\rho = \rho_0 e^{-h/h_s}$ where ρ_0 is the atmospheric density at sea level, h is the satellite altitude, and h_s is the atmospheric scale height. Also assume the atmosphere rotates with the Earth, so $\boldsymbol{V}_{rel} = \boldsymbol{v} - \boldsymbol{\omega}_E \times \boldsymbol{r}$ where $\boldsymbol{\omega}_E$ is the Earth's angular velocity. When written in matrix form, $\boldsymbol{V}_{rel} = \boldsymbol{v} - R_\omega \boldsymbol{r}$ where

$$R_\omega = \begin{bmatrix} 0 & -\omega_E & 0 \\ \omega_E & 0 & 0 \\ 0 & 0 & 0 \end{bmatrix} \tag{53}$$

So the acceleration due to atmospheric drag is given by

$$\boldsymbol{a}_{drag} = -\frac{\rho_0}{2\beta} e^{-h/h_s} V_{rel} \left(\dot{\boldsymbol{r}} - R_\omega \boldsymbol{r} \right) \tag{54}$$

4.5.4. Net Acceleration. The dynamic model is completed by combining all accelerations from the previous sections, $\boldsymbol{a} = \boldsymbol{a}_{geo} + \boldsymbol{a}_{J2} + \boldsymbol{a}_{sun} + \boldsymbol{a}_{moon} + \boldsymbol{a}_{drag}$. First, for simplification, define

$$k_1 = 1 + \frac{\mu_S}{\mu_E}\left(\frac{r}{d_S}\right)^3 + \frac{\mu_M}{\mu_E}\left(\frac{r}{d_M}\right)^3 - \frac{3}{2} J_2 \left(\frac{r_E}{r}\right)^2 \left(3\sin^2\phi - 1\right) \tag{55}$$

$$k_2 = 3\frac{J_2}{r}\left(\frac{r_E}{r}\right)^2 \sin\phi \tag{56}$$

$$k_3 = \frac{\rho_0}{2\beta} e^{-h/h_s} V_{rel} \tag{57}$$

Then, with *I* being the 3x3 identity matrix, the dynamic model to be used for orbit determination is given as

$$\boldsymbol{a} = \left[-\frac{\mu_E}{r^3}\left(k_1 I + k_2 R_\phi\right) + k_3 R_\omega \right] \boldsymbol{r} - k_3 \boldsymbol{v} \tag{58}$$

5. OBSERVABILITY ENHANCED GUIDANCE LAW (OEGL)

5.1. GUIDANCE LAW LOGIC

All guidance laws have the goal of driving the missile towards the target; the difference is how each law achieves that goal. The proportional navigation guidance law is based off the idea of eliminating the rotation in the line-of-site (LOS), augmented proportional navigation uses the same philosophy while assuming constant target acceleration, and the linear optimal guidance law is developed by formulating the guidance problem into an optimal control problem, and minimizing the miss distance while limiting the required missile acceleration.

The Observability Enhanced Guidance Law (OEGL), presented in this section, is designed to drive the missile to the target, just as other guidance laws, but it is to do so in such a way that the system observability is enhanced.

5.2. OBSERVABILITY METRIC

In order to enhance the system observability, it is required that a suitable metric be defined to quantify the system observability. For linear systems described by Equation 6, it can be shown that the system is completely observable if and only if the observability matrix, $O = [H^T \; A^{2T}H^T \; \ldots \; A^{nT}H^T]^T$, has full rank. Since the SDRE and θ-D filters require a linear-like structure, the system is locally observable if the local observability matrix, $O(x) = [H^T(x) \; A^{2T}(x)H^T(x) \; \ldots \; A^{nT}(x)H^T(x)]^T$, has full rank. Therefore a suitable metric for the system observability is $\Delta_o = \alpha\{|\det[O(x)]|\}$, where $\det(\cdot)$ is the matrix determinant, $|\cdot|$ is the absolute value function, and $\alpha(\cdot)$ is a strictly increasing function.

5.2.1. 2-D Engagement. To develop the OEGL, first consider the 2-D missile problem. The state dependant coefficient matrices, A(x) and H(x), are chosen to be

$$A(x)=\begin{bmatrix} 0 & 0 & 1 & 0 \\ 0 & 0 & 0 & 1 \\ \dot{\theta}^2 & 0 & 0 & 0 \\ 0 & 0 & -2\dot{\theta}/r & 0 \end{bmatrix} \tag{59}$$

$$H=\begin{bmatrix} 0 & 1 & 0 & 0 \end{bmatrix} \tag{60}$$

It is important to note that if $A_{31} = 0$, then the product HA^j, for any j, would have zeros in the first column and thus immediately cause $O(x)$ to be rank deficient. With a little effort, the determinant of the local observability matrix for this system is found to be

$$\det\left[O(x)\right]=4\left(\dot{\theta}^2/r\right)^2 \tag{61}$$

Therefore, the observability metric for this system is selected to be

$$\Delta_o=\dot{\theta}^2/r \tag{62}$$

5.2.2. Extension to 3-D. Notice that the numerator in Equation 62 is simply A_{31}, the term that must necessarily remain non-zero in order to maintain system observability. In a parallel fashion, the state dependant coefficient matrices for the 3-D system are

$$A(x)=\begin{bmatrix} 0 & 0 & 0 & 1 & 0 & 0 \\ 0 & 0 & 0 & 0 & 1 & 0 \\ 0 & 0 & 0 & 0 & 0 & 1 \\ \dot{\phi}^2+\dot{\theta}^2\cos^2\phi & 0 & 0 & 0 & 0 & 0 \\ 0 & 0 & 0 & -2\dot{\theta}/r & 0 & 2\dot{\theta}\tan\phi \\ 0 & 0 & 0 & -2\dot{\phi}/r & -\dot{\theta}\sin\phi\cos\phi & 0 \end{bmatrix} \tag{63}$$

$$H=\begin{bmatrix} 0 & 1 & 0 & 0 & 0 & 0 \\ 0 & 0 & 1 & 0 & 0 & 0 \end{bmatrix} \tag{64}$$

Notice again that if $A_{41} = 0$, the local observability matrix would be rank deficient because HA^j, for any j, would have zeros in the first column. By noting the similarity between the 2-D and 3-D cases, it can be reasonably assumed that a suitable observability metric for the 3-D system is

$$\Delta_o = \left(\dot{\phi}^2 + \dot{\theta}^2 \cos^2 \phi\right) / r \tag{65}$$

5.3. GUIDANCE LAW FORMULATION

The goal of any guidance law is to drive the relative range, r, to zero, and in order for that to happen, the LOS angular rate, $\dot{\theta}$, must decrease to zero. This indicates that the observability metric approaches an indeterminate value as the missile approaches the target. If $\dot{\theta}^2$ decreases faster than r, then the system becomes unobservable as Δ_o becomes zero, and if r decreases faster than $\dot{\theta}^2$, the filter may encounter numerical instability as Δ_o becomes infinite. As a result, the OEGL attempts to drive both $\dot{\theta}$ and r to zero simultaneously in such a way that Δ_o remains constant.

In order to find the accelerations needed to keep Δ_o constant, first multiply Equation 65 by r and differentiate to get

$$\Delta_o \dot{r} = 2\dot{\phi}\ddot{\phi} + 2\dot{\theta}\ddot{\theta}\cos^2\phi - 2\dot{\theta}^2\dot{\phi}\sin\phi\cos\phi \tag{66}$$

which, using the 3-D EOMs, becomes

$$\frac{5}{2}\Delta_o r\dot{r} = \dot{\phi}\left(a_{t_\phi} - a_{m_\phi}\right) + \dot{\theta}\cos\phi\left(a_{t_\theta} - a_{m_\theta}\right) \tag{67}$$

Thus, letting $a_{t_\theta} - a_{m_\theta} = 5\dot{r}\dot{\theta}\cos\phi/2$ and $a_{t_\phi} - a_{m_\phi} = 5\dot{r}\dot{\phi}/2$ will cause Δ_o to remain constant. There is still one acceleration component left to find: a_{m_r}. Consider the radial EOM

$$\ddot{r} = r\left(\dot{\theta}^2\cos^2\phi + \dot{\phi}^2\right) + a_{t_r} - a_{m_r} \tag{30}$$

Employing the feedback linearization control technique and using positive constants, k_1 and k_2, such that $k_2 < k_1^2$, letting $a_{t_r} - a_{m_r} = -r\left(\dot{\theta}^2\cos^2\phi + \dot{\phi}^2\right) - 2k_1\dot{r} - k_2 r$ will cause r to strictly decrease towards zero given that dr/dt is initially negative. Therefore the missile accelerations, using the OEGL, are found from

$$a_{m_r} = a_{t_r} + r\left(\dot{\theta}^2\cos^2\phi + \dot{\phi}^2\right) + 2k_1\dot{r} + k_2 r \tag{68.a}$$

$$a_{m_\theta} = a_{t_\theta} - 5\dot{r}\dot{\theta}\cos\phi/2 \tag{68.b}$$

$$a_{m_\phi} = a_{t_\phi} - 5\dot{r}\dot{\phi}/2 \tag{68.c}$$

5.4. DISCUSSION OF OEGL

It is interesting to note the similarity between the OEGL and the proportional navigation (ProNav) guidance law. In ProNav, the missile acceleration is proportional to the closing velocity and the LOS angular rate. In the OEGL, this is also true, assuming no target acceleration, with a proportionality constant of 5/2. One downside to the OEGL, is that the target acceleration, which is not accurately known in reality, is required. Despite this pitfall, initial results using the OEGL indicate excellent performance when the target acceleration is neglected altogether.

6. STAGGERED FILTER IMPLEMENTATION CONCEPT

6.1. CONTINUOUS FILTERS

A continuous filter, such as the θ-D filter, has dynamics that are dependent not only on the filter state, and time in some cases, but also on the current measurement. This is to say that in general

$$\dot{x} = f(x,t) = g\left[x,t,z(t)\right] \tag{69}$$

where x is the filter state, t is time, and z is the measurement at t. A problem with implementing a continuous filter is that the measurements are not known at all t, but instead are only known at discrete times, $t_{n\text{-}1}$, t_n, t_{n+1}, etc. The continuous filter implementation procedure proposed involves coupling a specific numerical integration scheme with the continuous filter so as to approximate the continuous filter in a discrete time sense. Two integration methods are presented herein.

6.2. RUNGE-KUTTA SECOND ORDER

The first numerical integrator considered is the Runge-Kutta, 2nd order (RK2) integrator. In this method, a given system state at t_n is propagated to t_{n+1} via the algebraic equations

$$k_1 = hf(x_n, t_n) \tag{70}$$

$$k_2 = hf(x_n + k_1, t_n + h) \tag{71}$$

$$x_{n+1} = x_n + (k_1 + k_2)/2 \tag{72}$$

where x_n and x_{n+1} are the filter states at t_n and t_{n+1}, respectively, and $h = t_{n+1} - t_n$. Notice that every time the forcing function, f, is evaluated, a measurement is needed via Equation 69, so by only propagating the filter states between measurement times, the

continuous filter can be approximately implemented in a discrete time sense to produce state estimates at the discrete measurement times.

To increase the accuracy of the filter, a higher order integrator can be used, but some care must be taken. This is addressed in the next section.

6.3. RUNGE-KUTTA FOURTH ORDER

The Runge-Kutta, 4th order (RK4) integrator is a very commonly used integrator for its balance between numerical accuracy and required computations. As a result, it poses as a prime candidate for the implementation of a continuous time filter in a discrete time sense. As will be seen shortly, however, some care must be taken when using this integrator.

When using the RK4 integrator, the state at t_n is propagated to the time t_{n+1} via the algebraic equations

$$k_1 = hf\left(x_n, t_n\right) \tag{73}$$

$$k_2 = hf\left(x_n + k_1/2, t_n + h/2\right) \tag{74}$$

$$k_3 = hf\left(x_n + k_2/2, t_n + h/2\right) \tag{75}$$

$$k_4 = hf\left(x_n + k_3, t_n + h\right) \tag{76}$$

$$x_{n+1} = x_n + \left(k_1 + 2k_2 + 2k_3 + k_4\right)/6 \tag{77}$$

where again x_n and x_{n+1} are the filter states at t_n and t_{n+1}, respectively, and $h = t_{n+1} - t_n$. Now consider what happens when the RK4 integrator is used to propagate state estimates between the discrete measurement times.

In Figure 6.1, the available measurements are marked by X's and the state estimates are marked by O's. Consider the case, indicated by the grey arrow, when the state estimate at t_n is known and the RK4 integrator is used to propagate the state to t_{n+1}. In this case a measurement is required at $t_{n+1/2} = t_n + h/2$, but a measurement at this time is unavailable. Now consider the line labeled x^1 where the RK4 is used to propagate the state to t_{n+2}, instead of t_{n+1}. In this case all required measurements are available for the

integration, but unfortunately the state at t_{n+1} is not estimated. This problem is corrected by introducing the concept of a staggered filter.

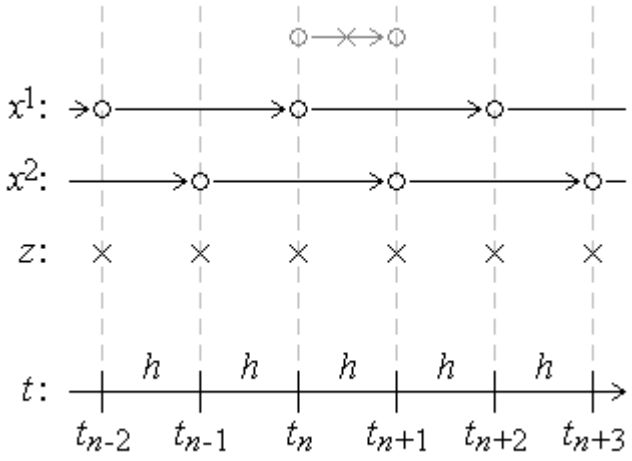

Figure 6.1. Staggered Filter Concept

Consider the case when two separate filters, indicated by lines x^1 and x^2, are used to propagate each state estimate between two measurement intervals. If the two filters are operated in a staggered fashion, as depicted in Figure 6.1, a state estimate is obtained at each measurement time, albeit from alternating filters. In the staggered filter concept, two identical filters are propagated independently of each other, but the filters share the available measurements. Using this staggered filter concept, it is possible to implement a continuous filter in a discrete time sense.

7. COMPUTER SIMULATION

7.1. OVERVIEW

This section describes the computer simulation used in this thesis. All programming was performed using the MATLAB software package, and a Runge-Kutta 4th order, fixed step size integration scheme was used to integrate the system EOMs. Figure 7.1 shows a flow diagram for the computer simulation.

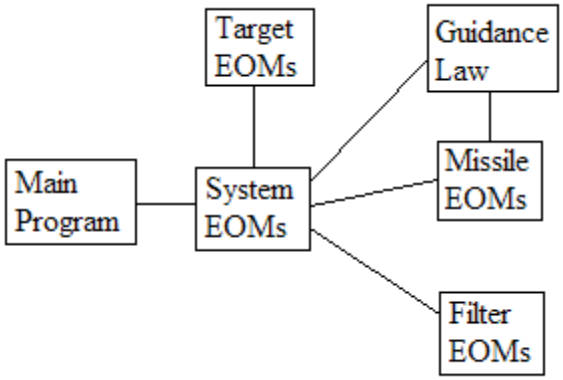

Figure 7.1. Computer Simulation Program Flow

The main program set the initial conditions for the missile, target, and filter states and initialized the selected filter (e. g. A_0 and C_0 for θ-D, P_0 for EKF, etc.). The main program then performs the numerical integration by sending the total system state vector (missile + target + filter) to the system EOMs function. Once the integration was completed, the main program performed post-processing calculations and plotted the simulation results.

When the system state vector is passed to the system EOMs, the target motion is calculated first as it is independent of the missile and filter motion. Next, the current filter states are sent to the guidance law to obtain the commanded acceleration, which is

then sent to the missile EOMs. Finally, the filter EOMs are computed and the entire system derivatives are returned to the main program for integration.

7.2. NOISE MODEL

As stated earlier, it is assumed that bearing only measurements are available. The measurement noise covariances for θ and ϕ are obtained from the target-sensor model

$$\sigma_\theta = \left(\sigma_{\theta_r}{}^2 / r^2 + \sigma_{\theta_0}{}^2 \right)^{1/2} \tag{78}$$

$$\sigma_\phi = \left(\sigma_{\phi_r}{}^2 / r^2 + \sigma_{\phi_0}{}^2 \right)^{1/2} \tag{79}$$

The first term represents the received signal power and varies inversely to the square of the range, *r*. The received power signal is analogous to "glint" for a radar-equipped missile system. The second term represents the uncertainty in the target position. In the case of a passive infrared sensor, the point of illumination may be shifted from its true location. Possible causes for this phenomenon include atmospheric refraction and electromagnetic interference (EMI). In the results to follow, $\sigma_{\theta,\mathrm{r}} = \sigma_{\phi,\mathrm{r}} = 0.0225$ rad^2 ft^2 and $\sigma_{\theta,0} = \sigma_{\phi,0} = 5.6\text{x}10^{-9}$ rad^2.

7.3. TARGET ACCELERATION MODEL

In the results that follow, the target maneuvers in a weaving fashion. The target's acceleration is modeled as

$$\boldsymbol{a}_t = a_{t_{\max}} \cos(\omega t)\, \boldsymbol{n} \tag{80}$$

where the maximum acceleration is set at 10g and the acceleration direction is

$$\boldsymbol{n} = \boldsymbol{k} \times \boldsymbol{v}_t / \left\| \boldsymbol{k} \times \boldsymbol{v}_t \right\| \tag{81}$$

The unit vector $\boldsymbol{k}$ points in the zenith direction and $\omega = 2\pi f$, where f is the target weave frequency.

7.4. MISS DISTANCE EVALUATION

In the missile engagement simulation a constant time step is used, but the point of closest approach most likely occurs in between time steps. In order to calculate the actual miss distance, Euler integration is used during the final time step, which is calculated in the following manner.

At the point of closest approach, the relative range vector is perpendicular to its derivative, so

$$0 = \boldsymbol{r}_k \cdot \dot{\boldsymbol{r}}_k = \left(\boldsymbol{r}_{k-1} + \dot{\boldsymbol{r}}_{k-1} \Delta t \right) \cdot \left(\dot{\boldsymbol{r}}_{k-1} + \ddot{\boldsymbol{r}}_{k-1} \Delta t \right) \tag{82}$$

where the relative position, velocity, and acceleration are known at time level k-1. The final time step is then calculated by solving the quadratic equation

$$\left(\dot{\boldsymbol{r}}_{k-1} \cdot \ddot{\boldsymbol{r}}_{k-1} \right) \Delta t^2 + \left(\dot{\boldsymbol{r}}_{k-1} \cdot \dot{\boldsymbol{r}}_{k-1} + \boldsymbol{r}_{k-1} \cdot \ddot{\boldsymbol{r}}_{k-1} \right) \Delta t + \left(\boldsymbol{r}_{k-1} \cdot \dot{\boldsymbol{r}}_{k-1} \right) = 0 \tag{83}$$

where the correct root is positive and less than the fixed simulation step size. The intercept simulation is run at the set time step until the estimated time to go is less than the fixed step size, at which point the above procedure is used to locate the point of closest approach.

7.5. FILTER PARAMETERS

The filter parameters used in this thesis are V = diag([.1 ft, 2 deg, 2 deg, .2 ft/s, 10 deg/s, 10 deg/s, 100 ft/s^2, 100 ft/s^2, 100 ft/s^2])^2, W = diag([10 deg, .1 deg])^2, and $\lambda_r = \lambda_\theta = \lambda_\phi = 2.5$. The state dependent coefficient matrices, used in the θ-D filter, were factored by using $A_0 = F(x_0)$ and $C_0 = H(x_0)$.

7.6. MONTE CARLO SIMULATIONS

Because random processes that are present in the missile-intercept problem, in order to fully evaluate the performance of a filter/guidance law combination, one needs to look at the expected value and covariance of the miss distance instead of just the miss distance of a single simulation. In the results presented in Section 7, Monte Carlo simulations were performed in order to estimate the expected value and covariance of the miss distance.

For each Monte Carlo simulation, 50 trial runs were performed for each engagement scenario, and the miss distance for each run was recorded. At the completion of the 50 trials, the miss distances were averaged to estimate the expected value of the miss distance, and the standard deviation of the finite set was used as the estimate for the miss distance covariance.

7.7. ORBIT SIMULATION

For the results presented in the next section, simulated measurements were created using a high fidelity orbit model incorporating the GRACE Gravity Model with degree and order 12, solar radiation pressure, atmospheric drag with the Harris-Priester atmospheric density model, and solar and lunar third-body gravitational effects. For the measurement model, it was assumed that the GPS receiver provides the global satellite point position measurement in the Earth-centered inertial reference frame at the J2000 epoch. While not all receivers provide these data directly, most provide enough information from which a small amount of preprocessing will produce the desired result.

For all figures presented in the next section, the satellite initial Keplerian orbital elements were set with a semimajor axis of 6778 km, an eccentricity of 0.01, and inclination of 45 degrees, 20 degrees for the right ascension of the ascending node (RAAN), and 50 degrees for the argument of periapsis. The initial true anomaly for the satellite was set at 100 degrees. The filter was initialized by applying Battin's method for solving Lambert's problem [48] to two measurements spaced one minute apart. After the filter was initialized, measurements with five meter precision were taken at a frequency of one Hertz. On the first stage of the RK4 filter, the RK2 integrator was used to stagger the two separate filters, after which the RK4 integrator was used as new measurements were taken.

The θ-D filter was tuned with $W = 10^{-9}I_6$ and $V = 25/3 \cdot 10^{-6}I_3$, where I_3 and I_6 are the 3x3 and 6x6 identity matrices, respectively. The disturbance terms were selected with $k_1 = 1.01$, $k_2 = 0.99$, and $l_1 = l_2 = 1$, where only the first three terms were used in calculating the approximate solution to the Riccati equation.

8. RESULTS AND CONCLUSIONS

8.1. 2-D RESULTS

The results presented in this subsection demonstrate the effectiveness of the θ-D filter coupled with the linear optimal guidance law (LOGL), when applied to the 2-D target-intercept problem. For the results presented in this subsection, unless otherwise stated, the initial position of the missile is the origin and the velocity is 4850 ft/s downrange and -8.4684 ft/s cross range. Also, the initial position of the target is 10000 ft downrange and -300 ft cross range, and the initial target velocity is 3000 ft/s downrange and 40 ft/s cross range.

8.1.1. θ-D Filter Performance. Figures 8.1-8.3 show the filter states compared to the actual states. The filter is able to estimate four of the six observer states. The filter inability to estimate the target acceleration is a result of not being able to accurately model the target acceleration as well as not being able to measure the acceleration.

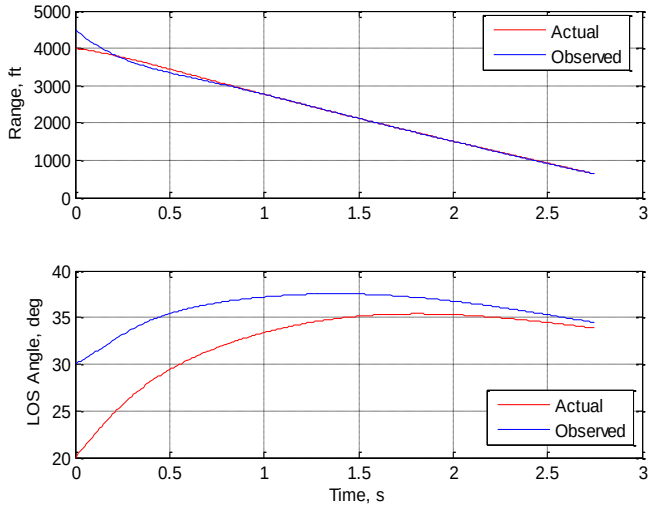

Figure 8.1. Estimates for r and θ

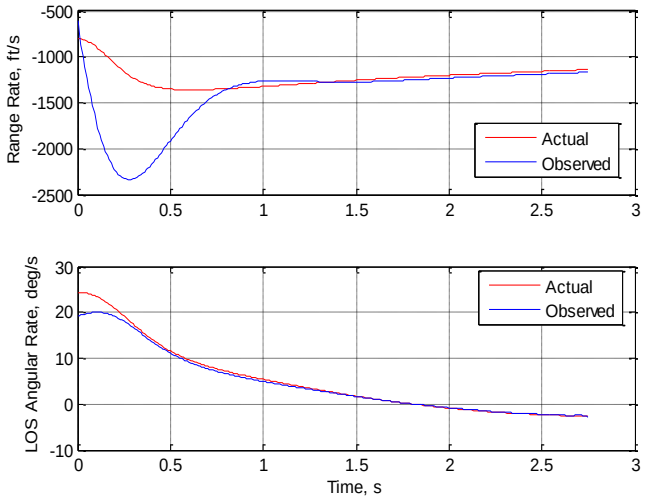

Figure 8.2. Estimates for $\dot{r}$ and $\dot{\theta}$

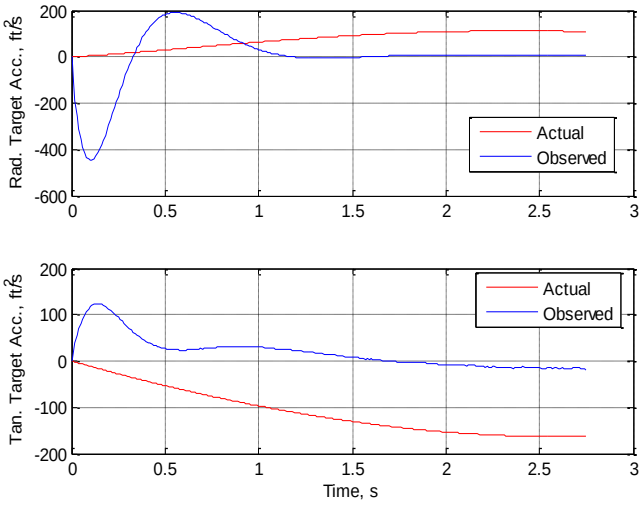

Figure 8.3. Estimates for Target Acceleration

8.1.2. Data Smoothing. Figures 8.4-8.6 show the same simulation as in Figs. 8.1-8.3, but with the addition of data smoothing. One result of the smoothing process is that many, if not all, of the system states are obtained from the polynomial fit. These

additional state estimates can be used to "reset" the filter states so as to eliminate initial filter mismatch. As can be seen in the figures, the estimator produces considerably better estimates with the addition of smoothing and state reset.

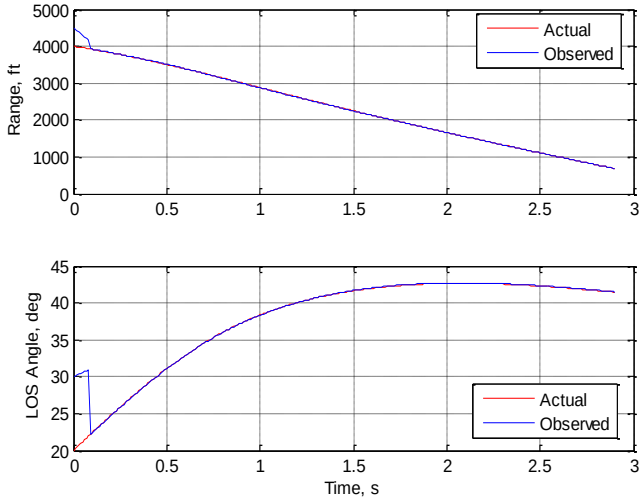

Figure 8.4. Estimates for r and θ with Smoothing and Reset

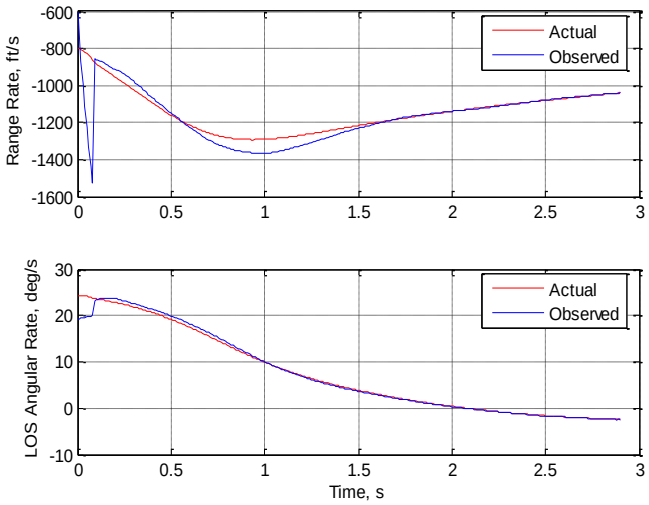

Figure 8.5. Estimates for $\dot{r}$ and $\dot{\theta}$ with Smoothing and Reset

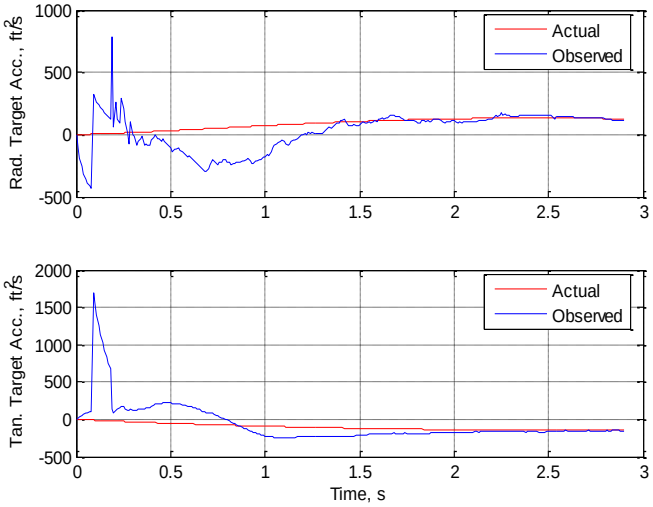

Figure 8.6. Estimates for Target Acceleration with Smoothing and Reset

8.2. 3-D RESULTS

The results presented in this subsection demonstrate the effectiveness of the θ-D filter coupled with the observability enhanced guidance law (OEGL), when applied to the 3-D target-intercept problem. For the results presented in this subsection, unless otherwise stated, the initial position of the missile is the origin and the velocity is 3800 ft/s downrange, 3800 ft/s cross range, and 3800 ft/s vertical. Also, the initial position of the target is 55000 ft downrange, 55000 ft cross range, and 55000 ft vertical, and the initial target velocity is -5000 ft/s downrange, -8200 ft/s cross range, and -2000 ft/s vertical. This corresponds to an initial range of approximately 95000 ft (or 29 km), an initial closing velocity of approximately 14300 ft/s (or 4.4 km/s), and an aspect angle of 3.77 degrees.

8.2.1. θ-D Filter Using Linear Optimal Guidance. Figures 8.7-8.12 show a typical simulation with a weave frequency of 1 Hz and using the Linear Optimal Guidance Law (LOGL) with data smoothing. The LOGL is summarized in Appendix B and the data smoothing procedure is found in Appendix C**.** Figures 8.8-8.10 show the filter estimates of the system states. The filter is able to accurately estimate the bearing angles as is to be expected since those are being measured. Figure 8.8 indicates that the filter is able to reasonably estimate the range and range rate with some errors beginning to occur as the missile nears the target. This is to be expected as the system is nearing a singularity in the EOM's and numerical instability becomes much more likely.

Without smoothing, the filter would estimate the target acceleration as approximately zero due to the first order Markov process used in the filter dynamics, but as can be seen in Figure 8.10 the smoothing process produces slightly better results for the target accelerations. Figure 8.11 shows the missile accelerations obtained from using the LOGL.

Finally, Figure 8.12 shows expected miss distances as the weave frequency is varied. The θ-D filter, when coupled with the LOGL, produces fairly consistent miss distances with a tendency to increase as the weave frequency increases.

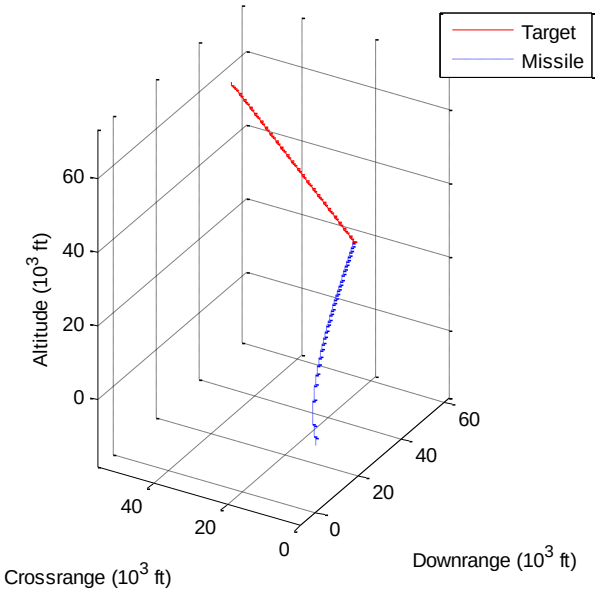

Figure 8.7. Missile Engagement Using LOGL

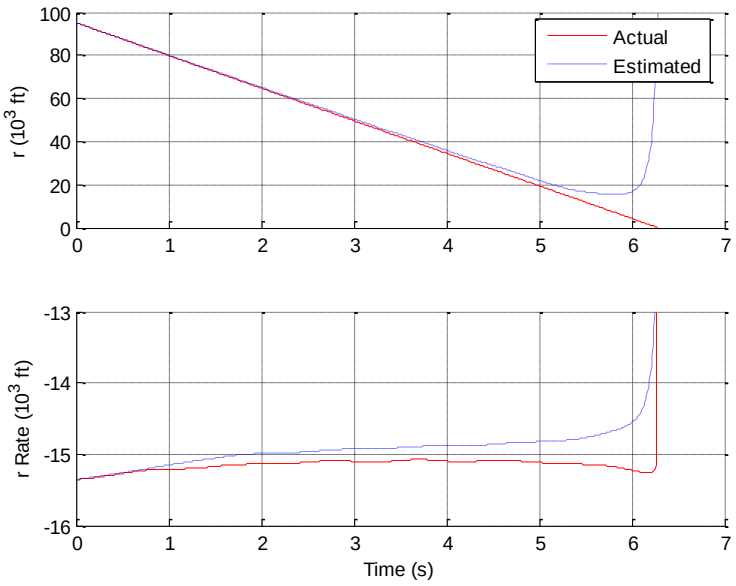

Figure 8.8. Range and Range Rate Estimates Using LOGL

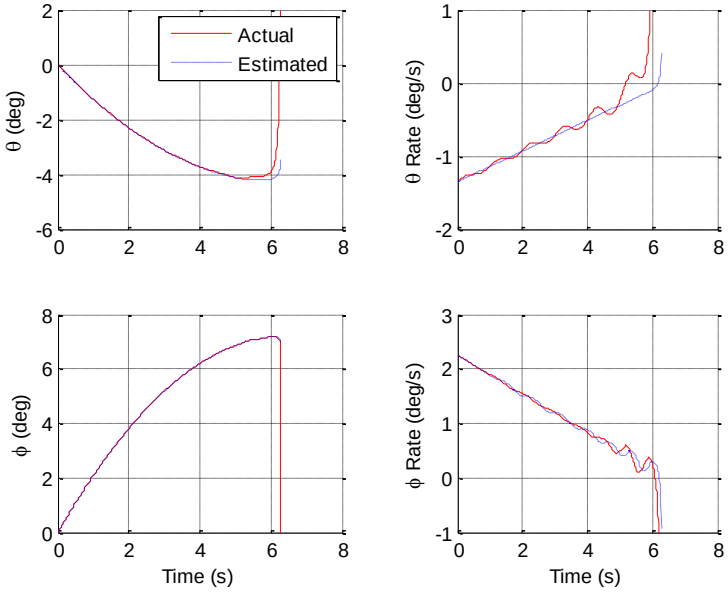

Figure 8.9. Bearing Angle Estimates Using LOGL

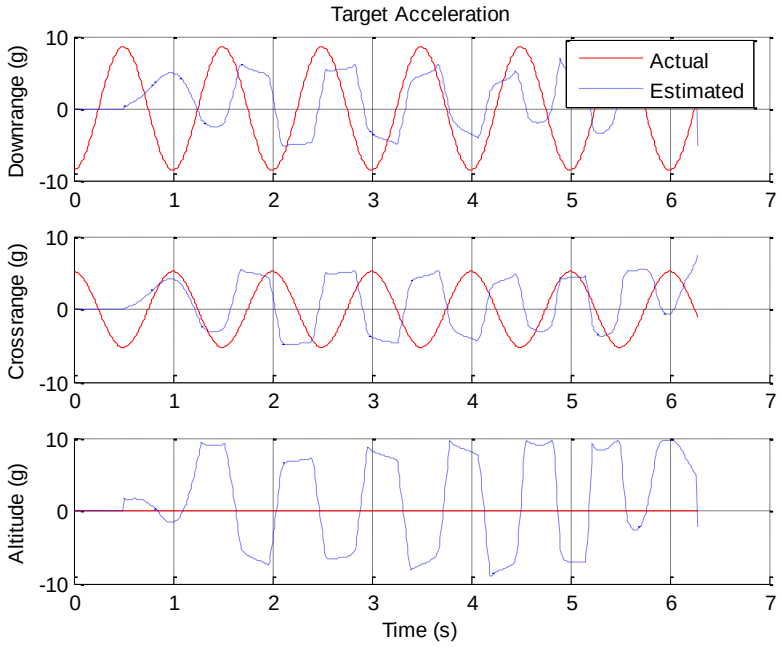

Figure 8.10. Target Acceleration Estimates Using LOGL

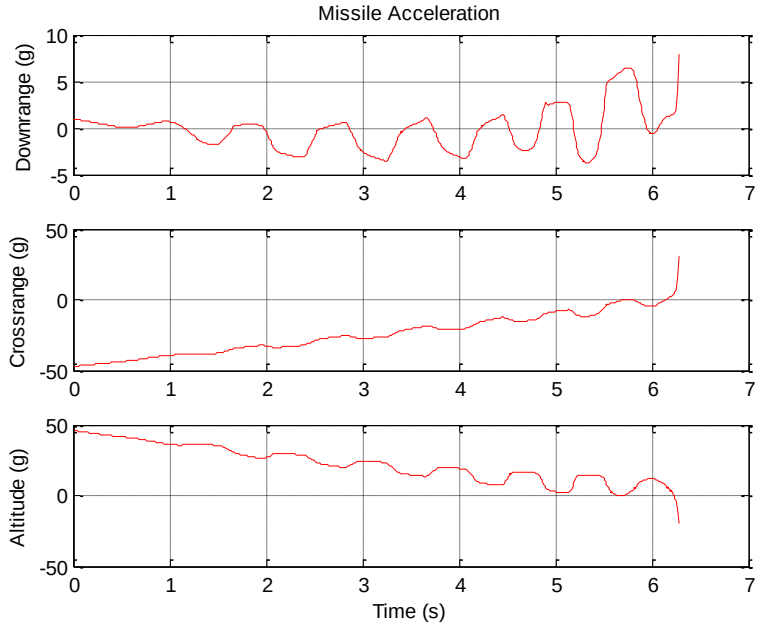

Figure 8.11. Missile Accelerations Using LOGL

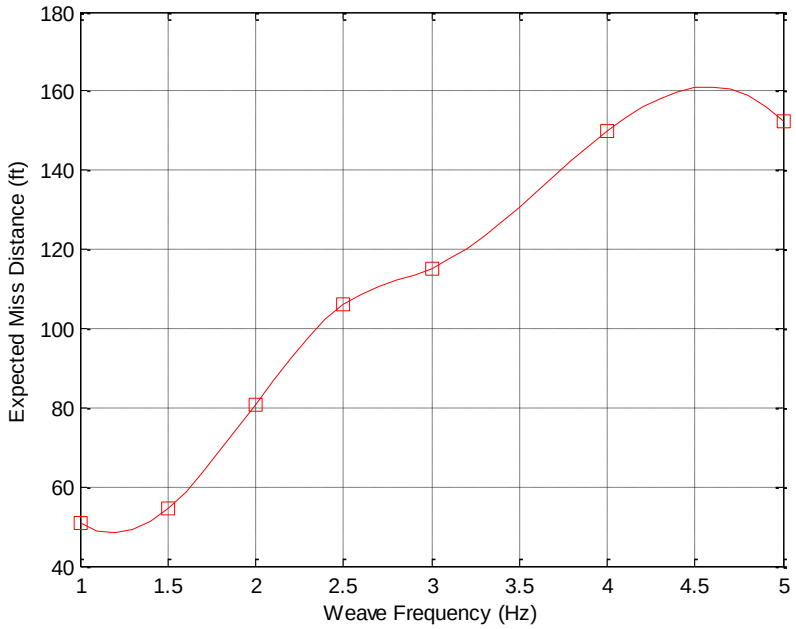

Figure 8.12. Expected Miss Distance Using LOGL

8.2.2. θ-D Filter Using Observability Enhanced Guidance. Figures 8.13-8.18 show a typical simulation with a weave frequency of 1 Hz and using the Observability Enhanced Guidance Law (OEGL). Comparison studies indicated that better results are obtained when the OEGL is used without the data smoothing process augmenting the filter. Figures **8.14**-8.16 show the filter estimates of the system states. The filter is able to accurately estimate the bearing angles as is to be expected since those are being measured. Furthermore, Figure 8.14 indicates that the filter is able to accurately estimate the range and range rate, more so than when using the LOGL.

Figure 8.17 shows the missile accelerations obtained from using the OEGL. Notice that the OEGL requires accelerations of the same magnitude as the LOGL. Finally, Figure 8.18 shows expected miss distances as the weave frequency is varied. The θ-D filter, when coupled with the OEGL, produces much smaller miss distances than does the filter coupled with the LOGL.

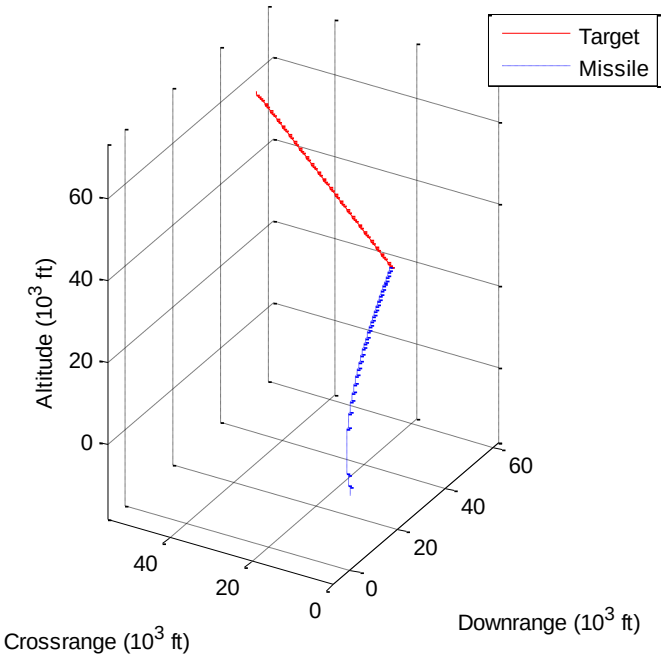

Figure 8.13. Missile Engagement Using OEGL

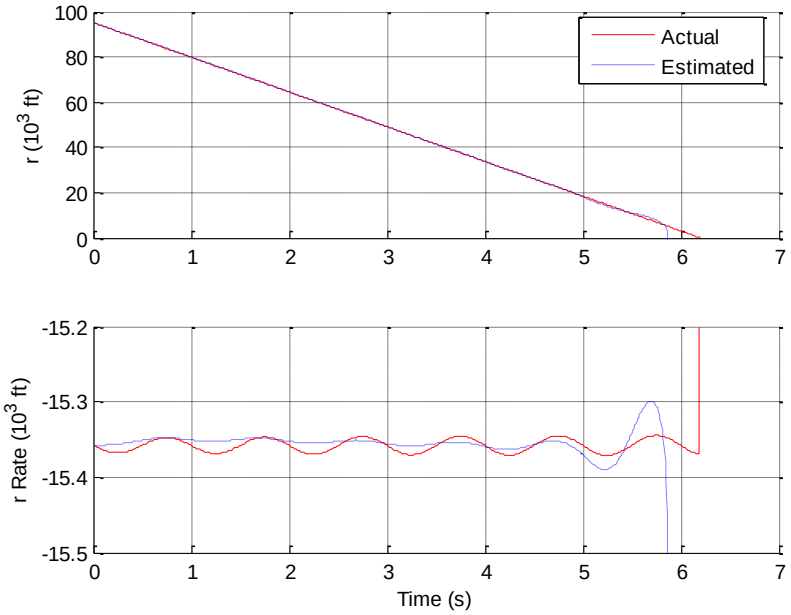

Figure 8.14. Range and Range Rate Estimates Using OEGL

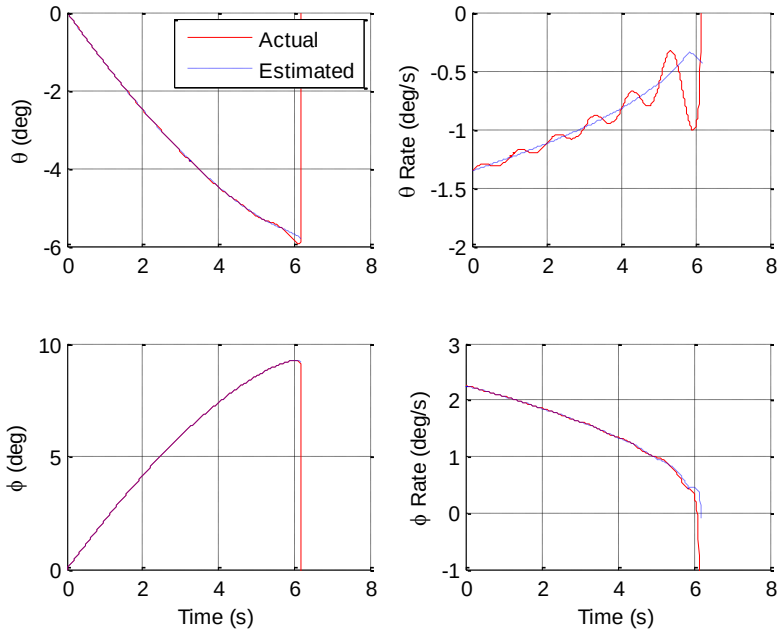

Figure 8.15. Bearing Angle Estimates Using OEGL

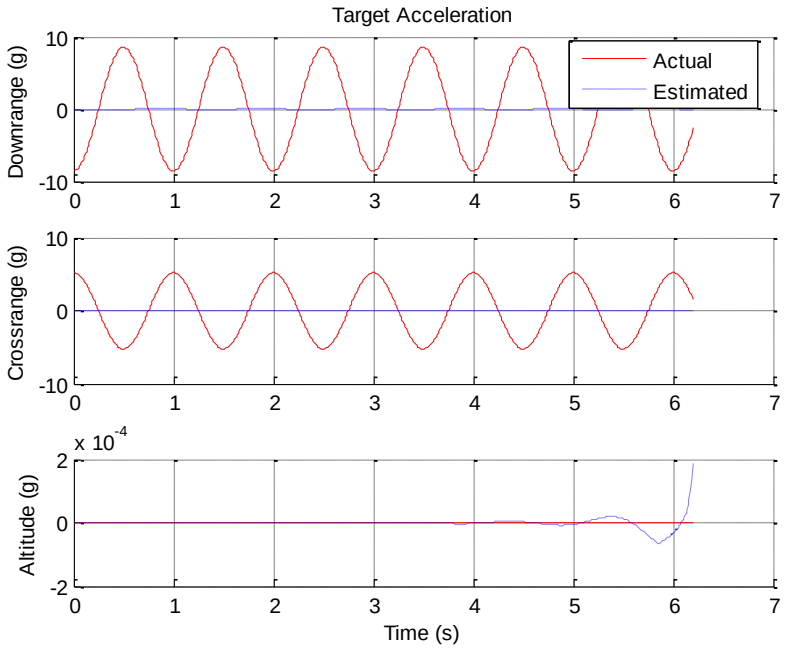

Figure 8.16. Target Acceleration Estimates Using OEGL

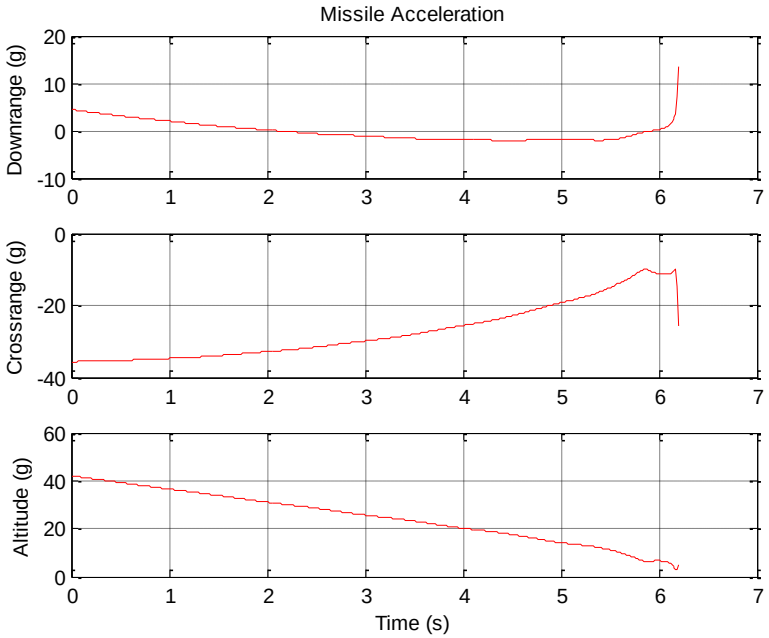

Figure 8.17. Missile Accelerations Using OEGL

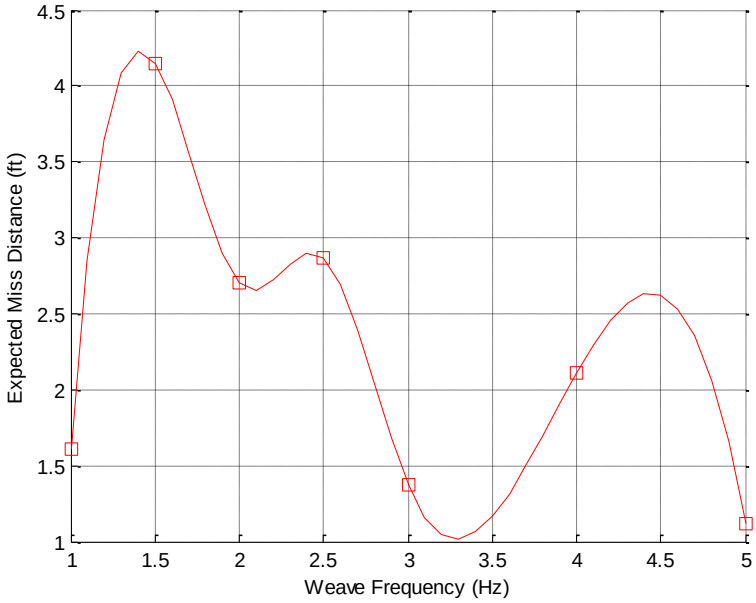

Figure 8.18. Expected Miss Distance Using OEGL

8.2.3. Expected Miss Distance Comparison. The expected miss distances, using the LOGL and OEGL, have been compared. The OEGL produces more consistent and smaller miss distances as weave frequency varies, as is shown in Table 7.1.

Table 7.1. Comparison of Expected Miss Distance

Weave Frequency (Hz)	Expected Miss Distance (ft)	
	LOGL	OEGL
1.0	51.04 ± 0.15	1.61 ± 0.01
1.5	54.65 ± 0.25	4.15 ± 0.40
2.0	80.82 ± 0.67	2.70 ± 0.01
2.5	106.05 ± 1.74	2.87 ± 2.15
3.0	115.23 ± 3.67	1.37 ± 0.26
4.0	149.80 ± 14.21	2.11 ± 1.72
5.0	152.34 ± 14.93	1.12 ± 0.99

8.2.4. Initial Heading Error Analysis. The effect of initial heading error on the expected miss distances using the θ-D filter and the Extended Kalman Filter (EKF) has been studied. The heading error is defined as the angle between the missile velocity and the direction to the predicted impact point (PIP). For this analysis, the missile velocity was rotated to a specified initial heading error while its position, along with the target position and velocity, remained fixed. The results are presented in Table 7.2.

Table 7.2. Heading Error Effect on Expected Miss Distance

Initial Heading Error (deg)	Expected Miss Distance (ft)	
	θ-D	EKF
5	1.45 ± 0.20	6.21 ± 0.00
10	2.09 ± 0.19	3.52 ± 3.37e-4
15	6.00 ± 0.01	0.75 ± 3.35e-4
20	5.90 ± 0.01	3.76 ± 4.85e-4
25	4.15 ± 0.00	5.76 ± 4.45e-4
30	309.53 ± 0.00	308.68 ± 0.01

The missile acceleration was limited to 30g's. It is clear that, as the initial heading error nears 30 degrees, the limit on the missile acceleration prohibits the missile from successfully turning onto the collision course.

8.3. ORBIT DETERMINATION RESULTS

This section provides results of the orbit determination algorithm consisting of the θ-D filter implemented using the Staggered Filter Concept. Results using the standard common EKF are also provided for comparison.

8.3.1. Staggered θ-D Filter with RK4 Integration. Figures 8.19-8.22 show the filter performance when using the staggered filter with RK4 integration. From the results it is evident that the θ-D filter, coupled with the RK4 integrator, is capable of estimating the satellite orbit after approximately 30 minutes. It is also evident that while the measurement accuracy was five meters, the staggered θ-D filter with RK4 integration is capable of obtaining approximately three meters of positional accuracy. It is clear from Figures 8.19 and 8.20 that the dynamic model used in the filter, coupled with the continuous nature of the θ-D filter, allows for accurate estimation of the shape and orientation of the satellite's orbit.

8.3.2. Extended Kalman Filter. For evaluation purposes, the staggered θ-D filter method was compared to a commonly used estimation method: the Extended Kalman Filter (EKF). For this method the filter dynamic model was propagated between the measurement times using RK4 integration and without measurement updates. In addition to state propagation an estimate for the error covariance was also propagated using

$$\dot{P} = PF^T + FP + W \tag{84}$$

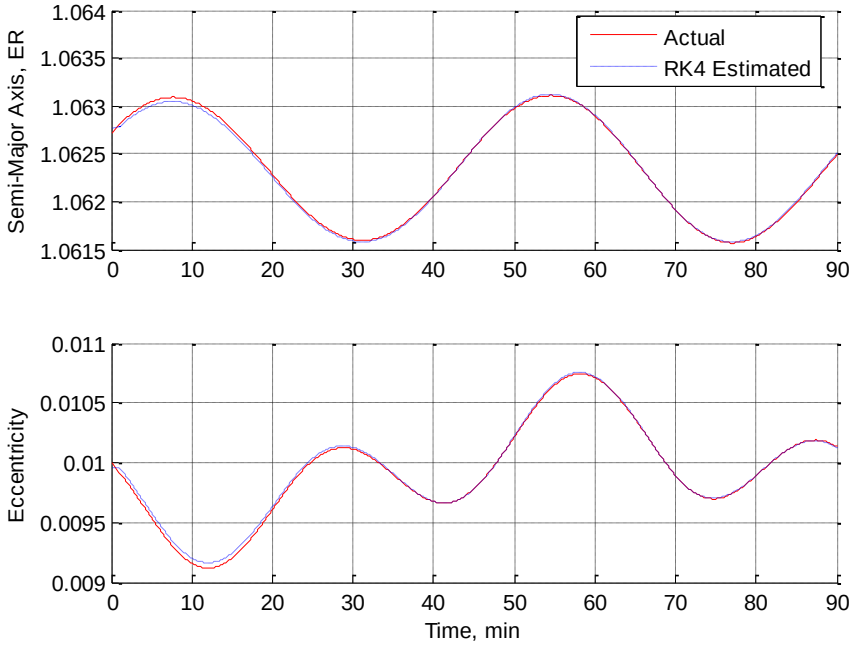

Figure 8.19. Orbital Shape Using RK4

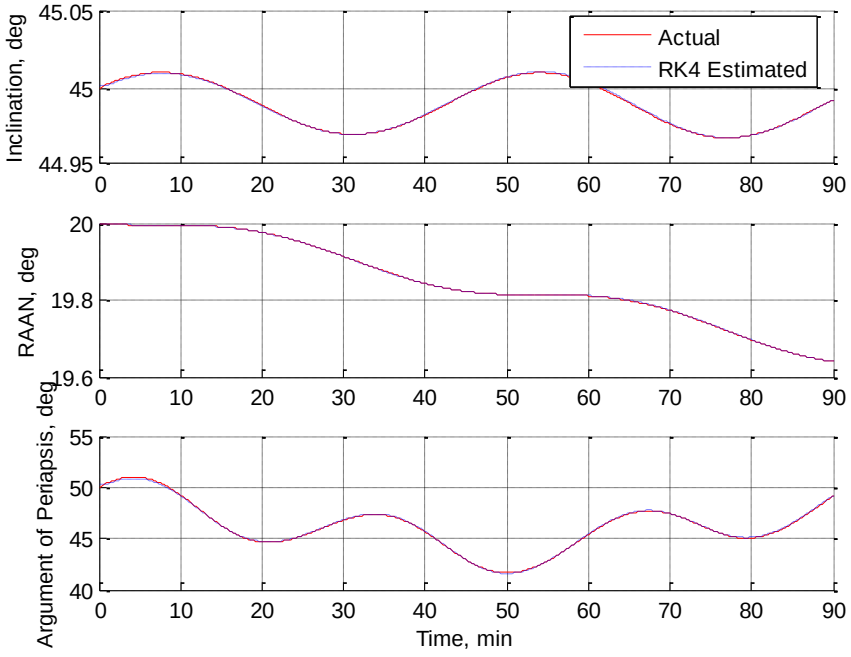

Figure 8.20. Orbital Orientation Using RK4

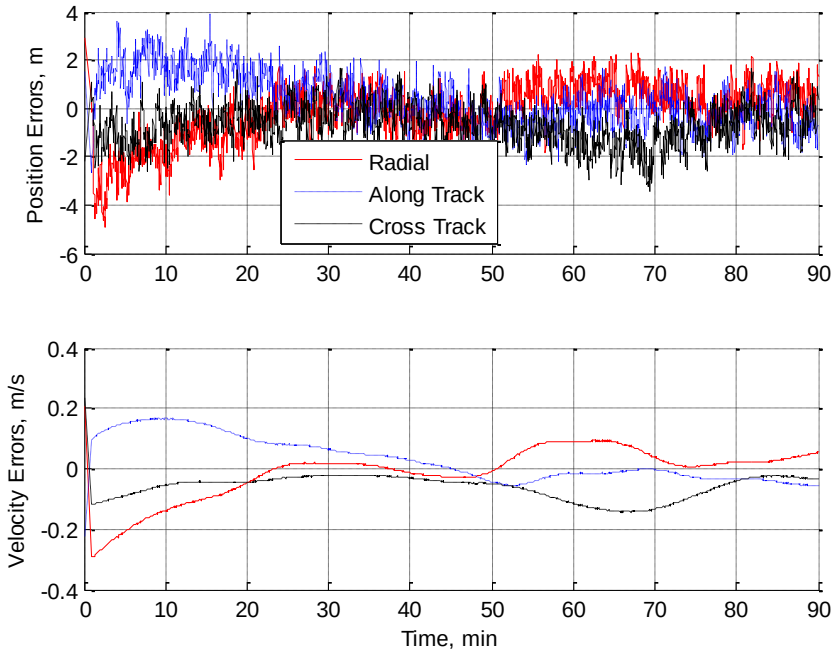

Figure 8.21. Filter Position/Velocity Errors Using RK4

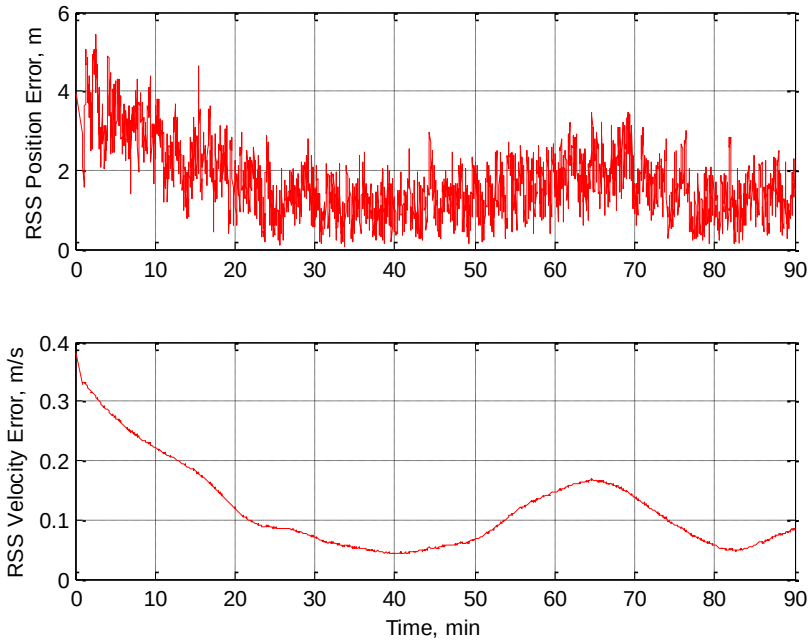

Figure 8.22. RSS Position/Velocity Errors Using RK4

where F is the gradient of the dynamic forcing function. At each measurement time, after the states were propagated, the state estimate and error covariance were updated using

$$\hat{x} = \bar{x} + K\left[z - H(\bar{x})\bar{x}\right] \tag{85}$$

$$\hat{P} = (I - KH)\bar{P} \tag{86}$$

where the filter gain, K, was calculated from

$$K = \bar{P}H^T\left(H\bar{P}H^T + V\right)^{-1} \tag{87}$$

In the EKF simulation, the initial error covariance estimate was set to $P = 10^2 I_6$. Figures 8.23-8.26 show the results for the EKF simulation. After approximately 5 minutes the EKF has reached its steady state with a position error standard deviation of approximate 5 meters. By comparing Figures 8.22 and 8.26 it is clear that while the EKF converges faster to steady state than does the θ-D, the proposed staggered θ-D filter achieves greater positional accuracy. It is also clear a similar trend occurs in the filter velocity estimates; however the additional velocity accuracy is not as pronounced as is the positional accuracy.

8.4. CONCLUSIONS

This thesis presented the θ-D filter formulation as applied to the 3D missile intercept problem. The simulations used in this study assumed a passive measurement system with bearing angles being the only measured data. Additionally, a comparison was made between the linear optimal guidance law and a different guidance law based on the idea of enhancing system observability. The results presented in this report indicate considerable promise for the use of the θ-D filter in the missile intercept problem.

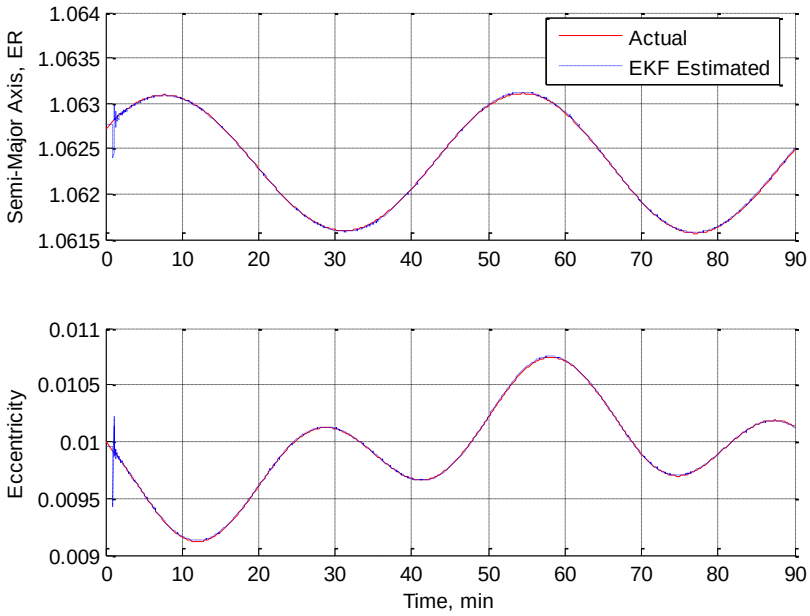

Figure 8.23. Orbital Shape Using EKF

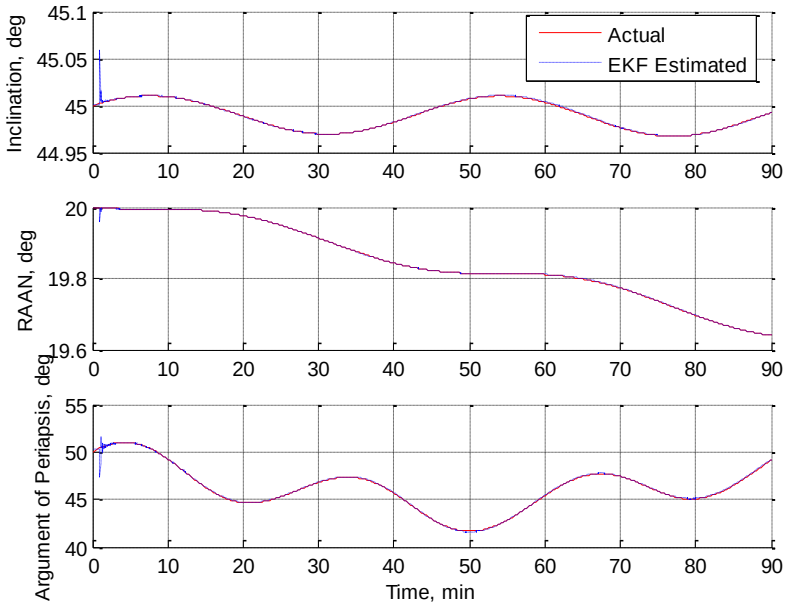

Figure 8.24. Orbital Orientation Using EKF

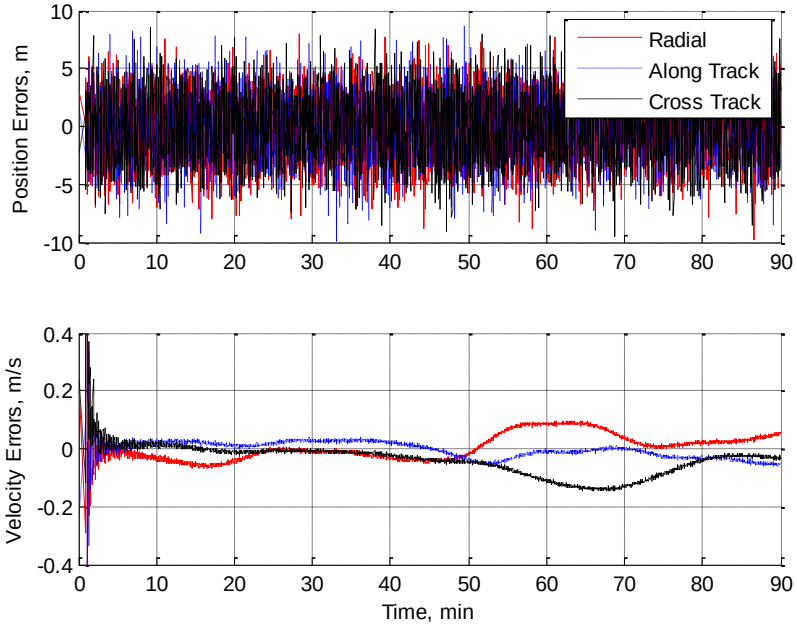

Figure 8.25. Filter Position/Velocity Errors Using EKF

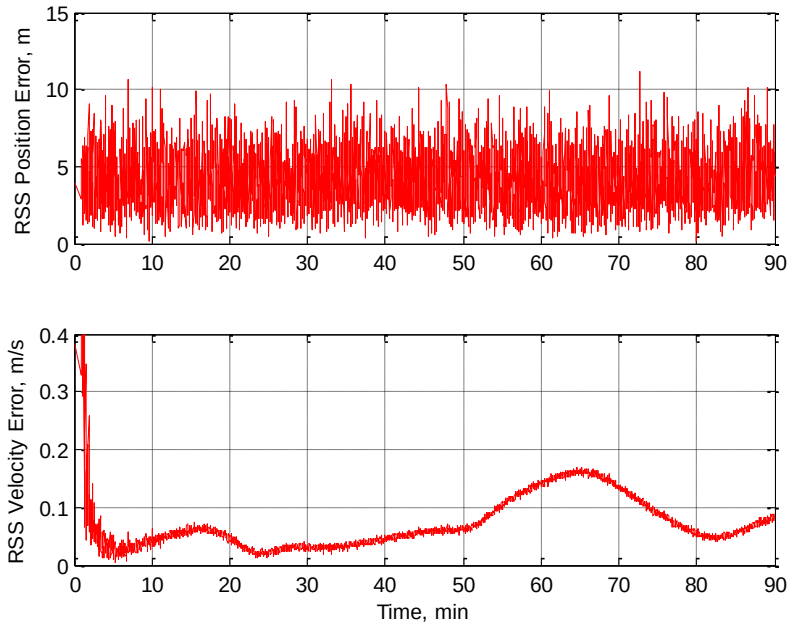

Figure 8.26. RSS Position/Velocity Errors Using EKF

Additionally, this thesis presented a novel orbit determination scheme that is set to be implemented aboard the Missouri S&T M-SAT mission. This method uses a new nonlinear filter, θ-D, that is implemented using the staggered filter concept. This combination allows the continuous θ-D filter to be implemented in a discrete time sense. This orbit determination scheme was compared to the commonly used Extended Kalman Filter and the results presented indicate that while the proposed scheme takes a little longer to converge, it arrives at a lower steady state RSS positional error.

APPENDIX A.
θ-D PROOF OF CONVERGENCE

In order to prove that the series $\Sigma_i T_i(x,\theta)\theta_i$ converges, it is convenient to eliminate the variable θ. This can be done by defining, $\hat{T}_i = T_i\theta^i$, after which Equations 22 become

$$0 = V + A_0\hat{T}_0 + \hat{T}_0A_0^T - \hat{T}_0C_0^TW^{-1}C_0\hat{T}_0 \tag{A1.0}$$

$$\begin{aligned}&\hat{T}_1\left(A_0 - \hat{T}_0C_0^TW^{-1}C_0\right)^T + \left(A_0 - \hat{T}_0C_0^TW^{-1}C_0\right)\hat{T}_1\\ &= -\hat{T}_0\left(A(\hat{x}) - \hat{T}_0C_0^TW^{-1}C(\hat{x})\right)^T - \left(A(\hat{x}) - \hat{T}_0C_0^TW^{-1}C(\hat{x})\right)\hat{T}_0 - D_1\end{aligned} \tag{A1.1}$$

$$\begin{aligned}&\hat{T}_2\left(A_0 - \hat{T}_0C_0^TW^{-1}C_0\right)^T + \left(A_0 - \hat{T}_0C_0^TW^{-1}C_0\right)\hat{T}_2\\ &= -\hat{T}_1\left(A(\hat{x}) - \hat{T}_0C_0^TW^{-1}C(\hat{x})\right)^T - \left(A(\hat{x}) - \hat{T}_0C_0^TW^{-1}C(\hat{x})\right)\hat{T}_1\\ &+\left(C_0\hat{T}_1 + C(\hat{x})\hat{T}_0\right)^TW^{-1}\left(C_0T_1 + C(\hat{x})\hat{T}_0\right) - D_2\end{aligned} \tag{A1.2}$$

$$\vdots \qquad\qquad \vdots$$

$$\begin{aligned}&\hat{T}_n\left(A_0 - \hat{T}_0C_0^TW^{-1}C_0\right)^T + \left(A_0 - \hat{T}_0C_0^TW^{-1}C_0\right)\hat{T}_n\\ &= -\hat{T}_{n-1}\left(A(\hat{x}) - \hat{T}_0C_0^TW^{-1}C(\hat{x})\right)^T - \left(A(\hat{x}) - \hat{T}_0C_0^TW^{-1}C(\hat{x})\right)\hat{T}_{n-1}\\ &+\sum_{j=1}^{n-1}\left(C_0\hat{T}_j + C(\hat{x})\hat{T}_{j-1}\right)^TW^{-1}\left(C_0\hat{T}_{n-j} + C(\hat{x})\hat{T}_{n-j-1}\right) - D_n\end{aligned} \tag{A1.n}$$

where the disturbance terms, D_i, are now chosen in the form

$$D_j(\hat{x}) = k_je^{-l_jt}\left(-\hat{T}_{j-1}A^T(\hat{x}) - A(\hat{x})\hat{T}_{j-1}\right) \tag{A2}$$

Now, if the series $\Sigma_i\hat{T}_i$ converges, then so does the series $\Sigma_i T_i(x,\theta)\theta_i$. Based on Weierstrass's Theorem[18], if a set of real numbers, S_i, exists such that $S_i \le \left\|\hat{T}_i\right\|$ for all i, $\|\cdot\|$ being the maxtrix norm, and the series $\Sigma\imath S\imath$ is a convergent series, then $\Sigma_i\hat{T}_i$ is also a convergent series.

Begin by considering a linear Lyapunov equation, $A^TP + PA = -Q$, where the matrix A is Hurwitz. The solution to this equation is bounded by[29]

$$\|P\| \le -\|Q\| / \left[2\lambda_{\max}\left(A_{sym}\right)\right] \tag{A3}$$

where $A_{sym} = (A + A^T)/2$. Given the selected disturbance terms, it can be shown that the norm of $\hat{T}_1$ is bounded by

$$\left\|\hat{T}_1\right\| \le 2CC_1\left|\varepsilon_1\right|\left\|\hat{T}_0\right\| \tag{A4}$$

where $\varepsilon_1 = 1 - k_1 e^{-l_1 t}$ and

$$C = -\lambda_{\max}\left[\left(A_0 - \hat{T}_0 C_0{}^T W^{-1} C_0\right) + \left(A_0 - \hat{T}_0 C_0{}^T W^{-1} C_0\right)^T\right]^{-1} \tag{A5}$$

$$C_A = \max_{\hat{x}} \left\|A\left(\hat{x}\right)\right\| \tag{A6}$$

$$C_C = \max_{\hat{x}} \left\|\hat{T}_0 C_0{}^T W^{-1} C\left(\hat{x}\right)\right\| \tag{A7}$$

$$C_1 = C_A + C_C / \left|\varepsilon_1\right| \tag{A8}$$

assuming $A(x)$ and $C(x)$ are bounded (true in most engineering applications). Continuing along the same line, the bound on $\left\|\hat{T}_2\right\|$ is

$$\left\|\hat{T}_2\right\| \le 4C^2 C_1 C_2 \left|\varepsilon_1\right|\left|\varepsilon_2\right|\left\|\hat{T}_0\right\| \tag{A9}$$

where

$$C_0 = \left\| C_0^{\,T} W^{-1} C_0 \right\| \tag{A10}$$

$$C_B = \max_{\hat{x}} \left\| C^T(\hat{x}) W^{-1} C(\hat{x}) \right\| \tag{A11}$$

$$C_2 = \left(C_A + 2C_C\right)/C_1 |\varepsilon_1||\varepsilon_2| + C_0/2|\varepsilon_2| + C_B/4CC_1|\varepsilon_1||\varepsilon_2| \tag{A12}$$

In a similar fashion, one can show that

$$\left\|\hat{T}_n\right\| \le 2^n C^n C_1 \ldots C_n |\varepsilon_1| \ldots |\varepsilon_n| \left\|\hat{T}_0\right\| \tag{A13}$$

Letting $S_n = 2^n C^n C_1 \ldots C_n |\varepsilon_1| \ldots |\varepsilon_n| \left\|\hat{T}_0\right\|$ implies that $S_n/S_{n\text{-}1} = 2CC_n|\varepsilon_n|$, so in order for the series S_iS_i to converge, $2CC_n|\varepsilon_n| < 1$. Therefore, by choosing the parameters k_n and l_n so that $|\varepsilon_n| < 1/2CC_n$, will guarantee convergence of $\Sigma_i T_i(x,\theta)\theta_i$.

APPENDIX B.
LINEAR OPTIMAL GUIDANCE LAW

The linear optimal guidance law (LOGL) is derived in the following manner. Consider the 1-D intercept geometry shown in Figure B.1. The direction, r_0, corresponds to the initial line-of-sight (LOS) and r is the current relative range.

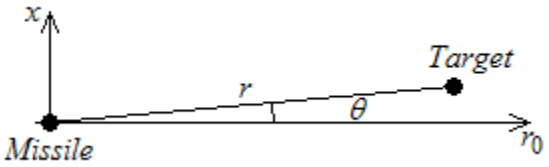

Figure B.1. 1-D Engagement Scenario

The goal is to find the missile acceleration, a_{m_x}, that minimizes the cost function,

$$J = \left(r_x \big|_{t_{go}} \right)^2 + \gamma \int_0^{t_{go}} a_x{}^2 dt \tag{B1}$$

where the first term minimizes the miss distance, the second term minimizes the energy input to the system, and t_{go} is the time remaining until the point of closest approach (PCA). The value, t_{go}, can be estimated as $t_{go} \approx \left| r / \dot{r} \right|$. The dynamic equations for the system are given by

$$\begin{bmatrix} \dot{r}_x \\ \dot{v}_x \\ \dot{a}_{t_x} \end{bmatrix} = \begin{bmatrix} 0 & 1 & 0 \\ 0 & 0 & 1 \\ 0 & 0 & -\lambda_x \end{bmatrix} \begin{bmatrix} r_x \\ v_x \\ a_{t_x} \end{bmatrix} + \begin{bmatrix} 0 \\ -1 \\ 0 \end{bmatrix} a_{m_x} \tag{B2}$$

where the target acceleration has been modeled as a first order Markov process using λ_x. The solution to this optimal control problem is

$$a_{m_x} = C_1 r_x + C_2 v_x + C_3 a_{t_x} \tag{B3}$$

where $N = 3t_{go}^{\ 3}/(3\gamma + t_{go}^{\ 3})$ and

$$C_1 = N / t_{go}^{\ 2} \tag{B4}$$

$$C_1 = N / t_{go} \tag{B5}$$

$$C_3 = N\left(e^{-\lambda_x t_{go}} + \lambda_x t_{go} - 1\right) / \left(\lambda_x t_{go}\right)^2 \tag{B6}$$

This concept can easily be extended to 3-D. The missile acceleration using the LOGL is then

$$a_m = C_r r + C_v v + C_{a_t} a_t \tag{B7}$$

where $C_r = C_1 I$ and $C_v = C_2 I$, I being the 3x3 identity matrix, and

$$C_{a_t} = \begin{bmatrix} C_{a_x} & 0 & 0 \\ 0 & C_{a_y} & 0 \\ 0 & 0 & C_{a_z} \end{bmatrix} \tag{B8}$$

$$C_{a_{(\cdot)}} = N\left(e^{-\lambda_{(\cdot)} t_{go}} + \lambda_{(\cdot)} t_{go} - 1\right) / \left(\lambda_{(\cdot)} t_{go}\right)^2 \tag{B9}$$

where $(\cdot) = x, y, z$.

APPENDIX C.
DATA SMOOTHING

Since nearly every guidance law requires some knowledge of the target acceleration, a technique has been applied to the filtering process that utilizes the system dynamics to augment the filter estimate of the target acceleration.

For the 3-D equations of motion, the target acceleration is given by

$$a_{t_r} = \ddot{r} - r\left(\dot{\theta}^2 \cos^2\phi + \dot{\phi}^2\right) + a_{m_r} \tag{C1}$$

$$a_{t_\theta} = r\ddot{\theta}\cos\phi + 2\dot{r}\dot{\theta}\cos\phi - 2r\dot{\theta}\dot{\phi}\sin\phi + a_{m_\theta} \tag{C2}$$

$$a_{t_\phi} = r\ddot{\phi} + r\dot{\theta}^2 \sin\phi\cos\phi + 2\dot{r}\dot{\phi} + a_{m_\phi} \tag{C3}$$

It is assumed that the acceleration of the missile is known. In order to calculate the target acceleration, estimates of d^2r/dt^2, $d^2\theta/dt^2$, and $d^2\phi/dt^2$ are needed. To obtain these estimates, a polynomial is fitted, in a least squares sense, to the filter data.

For a set time window in the past, $\Gamma = \{t_k\ t_{k-1}\ t_{k-2}\ \ldots\ t_{k-n}\}$, the filter state estimates, r, θ, and ϕ, at those times are recorded. Then a polynomial, $s = \Sigma_i a_i t^i$ for $i = 0, 1, \ldots, m \leq n + 1$, where $s \in \{r\ \theta\ \phi\}$, is fit to the data $s|_\Gamma$ so as to minimize

$$J = \left(S - Ta\right)^T \left(S - Ta\right) \tag{C4}$$

where $S = s|_\Gamma$, $a = [a_0\ a_1\ a_2\ \ldots\ a_m]^T$, and

$$T = \begin{bmatrix} t_k^{\,0} & t_k^{\,1} & \cdots & t_k^{\,m} \\ t_{k-1}^{\,0} & t_{k-1}^{\,1} & \cdots & t_{k-1}^{\,m} \\ \vdots & \vdots & \ddots & \vdots \\ t_{k-n}^{\,0} & t_{k-n}^{\,1} & \cdots & t_{k-n}^{\,m} \end{bmatrix} \tag{C5}$$

The polynomial coefficients are calculated as

$$a = \left(T^T T\right)^{-1} T^T S \tag{C6}$$

The approximation polynomial can now be differentiated as needed to obtain the required estimates for calculating the target acceleration.

An alternate approach to the data smoothing is to perform the smoothing in Cartesian coordinates instead of spherical coordinates. The reason for doing so is that errors encountered through the smoothing process using spherical coordinates become magnified when substituted into Equations C1-C3. To remedy this, the states, $\{r\ \theta\ \phi\}$, are converted to $\{x\ y\ z\}$, and the least squares fit is applied to the Cartesian coordinates. Then the target acceleration can be estimated using

$$a_{t_x} = \ddot{x} + a_{m_x} \tag{C7}$$

$$a_{t_y} = \ddot{y} + a_{m_y} \tag{C8}$$

$$a_{t_z} = \ddot{z} + a_{m_z} \tag{C9}$$

Then the target acceleration is converted back to spherical coordinates using a simple rotation.

One note to consider is that sensor measurements, instead of filter states, should be used in the data smoothing process whenever possible. Doing so eliminates the effect of filter mismatch that may exist initially in the system.

BIBLIOGRAPHY

[1] Anderson, G. M., "Comparison of Optimal Control and Differential Game Intercept Missile Guidance Laws," *Journal of Guidance and Control*, Vol. 4, No. 2, March-April, 1981.

[2] Babu, K., Sarma, I., and Swamy, K., "Switched Bias Proportional Navigation for Homing Guidance Against Highly Maneuvering Target," *Journal of Guidance, Control and Dynamics*, 17(6), 1994, pp. 1357-1363.

[3] Balakrishnan, S. N. and Speyer, J. L., "Assumed Density Filter with Application to Homing Missile Guidance," AIAA Journal of Guidance, Control and Dynamics, January-February 1989, pp. 4-12.

[4] Balakrishnan, S. N. and Speyer, J. L., "Coordination based Filter for Improved target tracking," AIAA Journal of Guidance and Control, vol. 9, no.6, nov.-Dec.-1986,pp. 704-709.

[5] Ben-Asher, J. Z. and Levinson, S., "Trajectory Shaping in Linear-Quadratic Pursuit-Evasion Games," JGCD, No. 6, 2004.

[6] Blakelock, J.H., "Automatic Control of Aircraft and Missiles," Wiley, New York,1991.

[7] Brierly, S. D., and Longchamp, R., "Application of Sliding Mode Control to Air-Air Interception Problem," *IEEE Transaction on Aerospace and Electronic Systems*, 2, 1990, pp. 306-325.

[8] Bryson, A. E. and Ho, Y. C., "Applied Optimal Control," Hemisphere Publishing Co., New York 1975.

[9] Cloutier, J. R., D'Souza, C.N. and Mracek, C.P., "Nonlinear Regulation and Nonlinear H_∞ Control Via the State-Dependent Riccati Equation Technique", *Proceedings of the first International Conference On Nonlinear Problems in Aviation and Aerospace*, Daytona Beach,FL, May 1996.

[10] Cloutier, J. R., Evers, J. H. and Feely, J. J., "Assessment of Air-to-Air Missile Guidance and Control Technology," *IEEE Control Systems Magazine*, October 1989, pp. 27-34.

[11] Cloutier, J. R. and Stansbery, D.T., "Nonlinear, Hybrid Bank-to-Turn/Skid-to-Turn Missile Autopilot Design," AIAA Guidance, Navigation, and Control Conference and Exhibit, Aug. 6-9, Montreal, Canada, 2001.

[12] Cloutier, J. R., "Time-To-Go-Less Guidance With Cross-Channel Couplings," AIAA Missile System Conference, 1999.

[13] Deutschmann, J. K. and Bar-Itzhack, I. Y., "Evaluation of Attitude and Orbit Estimation Using Actual Earth Magnetic Field Data," *Journal of Guidance, Control, and Dynamics*, Vol. 24, No. 3, 2001.

[14] D'Souza, C.N., McClure, M.A. and Cloutier, J.R., "Spherical Target State Estimators," *Proceedings of the American Control Conference*, Baltimore, Maryland, June, 1994.

[15] Edwards, C. and Spurgeon, S., *Sliding Mode Control*, Taylor & Francis, Bristol, PA, 1998

[16] Evers, J.H., Cloutier, J.R., Lin, C.F., Yueh, W.R., and Wang, Q., "Application of Integrated Guidance and Control Schemes to a Precision Guided Missile," *Proceedings of American Control Conference*, pp. 3225-3230, 1992.

[17] Hall, K. R. "Development and Comparison of estimation Algorithms for Airborne Missiles", AFATL-TR-84-47, May 1984.

[18] Korn, G. A. and Korn, T. M., *Mathematical Handbook For Scientists and Engineers*, Dover Publications, Inc., New York, 2000.

[19] Krupp, D., Shkolnikov, I. A., and Shtessel, Y. B., "2-Slidng Mode Control for Nonlinear Plants with Parametric and Dynamic Uncertainties," *Proceedings of AIAA Guidance, Navigation, and Control Conference,* Denver, CO, AIAA paper No. 2000-3965, 2000.

[20] Lechevin, N. and Rabbath, C. A., "Lyapunov-Based Nonlinear Missile Guidance," *Journal of Guidance, Control, and Dynamics*, No. 6, 2004.

[21] Lee, S., Schutz, B. E., and Abusali, P. A. M., "Hybrid Precise Orbit Determination Strategy by Global Positioning System Tracking," *Journal of Spacecraft and Rockets*, Vol. 41, No. 6, 2004.

[22] Leung, S. and Montenbruck, O., "Real-Time Navigation of Formation-Flying Spacecraft Using Global-Positioning-System Measurements," *Journal of Guidance, Control, and Dynamics*, Vol. 28, No. 2, 2005.

[23] Levant, A., "Higher-Order Sliding Modes, Differentiation and Output-Feedback Control," *International Journal of Control*, *76*, 9/10, 2003, pp. 924-941.

[24] Lin, C.F. and Yueh, W.R., "Optimal Controller for Homing Missiles," *Proceedings of American Control Conference*, 1984.

[25] Maybeck,P.S. and Hentz, K.P.," Investigation of Moving bank Multiple Model Adaptive Algorithms," *AIAA Journal of Guidance and Control*, Vol. 10, No.1, Jan.-Feb., 1987, pp.90-96.

[26] Menon, P. K. and Ohlmeyer, E. J., "Integrated Design of Agile Missile Guidance and Control Systems," *Proceedings of the 7th Mediterranean Conference on Control and Automation*, Haifa, Israel, June 28-30, 1999.

[27] Menon, P. K. and Ohlmeyer, E. J., "Nonlinear Integrated Guidance and Control Laws For Homing Missiles," *AIAA Guidance, Navigation and Control Conference and Exhibit*, Montreal, Canada, August 6-8, 2001.

[28] Moon, J. and Kim, Y., "Design of missile guidance law via variable structure control," *Proceedings of AIAA Guidance, Navigation and Control Conference*, Denver, CO, 2000, Paper AIAA-2000-4068.

[29] Mori, T. and Derese, I. A., "A Brief Summary of the Bounds on the Solution of the Algebraic Matrix Equations in Control Theory," *International Journal of Control*, 1984, Vol. 39, No. 2, pp. 247-256.

[30] Ohlmeyer, E. J., "Standard Missile Guidance Laws," NSWCDD Internal Report, Code G23, Naval Surface Warfare Center, Dahlgren Division, Dahlgren, VA, April 1994.

[31] Oshman, Y. and Arad, D., "Enhanced Air-to-Air Missile Tracking Using Target Orientation Observations," *Journal of Guidance, Control, and Dynamics*, No. 4, 2004.

[32] Palumbo, N.F. and Jackson, T.D., "Development of a Fully Integrated Missile Guidance and Control System: A State Dependent Riccati Differential Equation Approach," *Proceedings of the IEEE Conference on Control Applications*, Hawaii, HI, August, 1999.

[33] Psiaki, M. L., “Satellite Orbit Determination Using a Single-Channel Global Positioning System Receiver,” *Proceedings of the 2000 AIAA/AAS Astrodynamics Specialist Conference*, August 14-17, Denver, CO, 2000.

[34] Raju, P. A. and Ghose, D., “Empirical Virtual Sliding Target Guidance Law Design: An Aerodynamic Approach,” IEEE-T-AES, No.4, Oct. 2003.

[35] Savkin, A. V., Pathirana, F. N., and Faruqi, F. A., “Problem of Precision Missile Guidance: LOR and H_∞ Control Framework,” IEEE-T-AES, No.3, Jul. 2003.

[36] Shkolnikov, I. A., Shtessel, Y. B., and Lianos, D. P., “Integrated Guidance-Control System of a Homing Interceptor: Sliding Mode Approach,” *Proceedings of AIAA Guidance, Navigation, and Control Conference*, Montreal, AIAA Paper # 2001-4218, Canada, August, 2001.

[37] Shkolnikov, I., Shtessel, Y., and Lianos, D., "The effect of sliding mode observers in the homing guidance loop," *IMechE Journal on Aerospace Engineering, Part G*, Vol. 219, No. 2, 2005, pp. 103-111.

[38] Shkolnikov, I. A., Shtessel, Y. B., Lianos, D. B., and Thies, A. T., “Robust Missile Autopilot Design via High-Order Sliding Mode Control,” *Proceedings of AIAA Guidance, Navigation, and Control Conference*, Denver, CO, AIAA paper No. -2000-3968, 2000.

[39] Shtessel, Y., Buffington, J., and Banda, S., "Multiple Time Scale Flight Control Using Re-configurable Sliding Modes," *AIAA Journal on Guidance, Control, and Dynamics*, vol. 22, No. 6, pp. 873-883, 1999.

[40] Shtessel, Y. B., Shkolnikov, I. A., and Brown, M. D. J., "An Asymptotic Second Order Smooth Sliding Mode Control," *Asian Journal of Control*, Vol. 5, No 4, 2003, pp. 498-504.

[41] Shtessel, Y., Shkolnikov, I., and Levant, A., "Missile Interceptor Guidance and Control Using Second Order Sliding Modes," *Proceedings of IFAC World Congress*, Prague, Czech Republic, 2005.

[42] Singer, R. A., "Estimating Optimal Tracking Filter performance For Manned maneuvering Targets," IEEE transactions on Aerospace Electronics Systems, vol. AES-15, n0.3, may 1969, pp.448-456.

[43] Slotine, J-J.E. and Li, W., *Applied Nonlinear Control*, Prentice Hall, Englewood Cliffs, NJ, 1991.

[44] Song, T.L. and Speyer, J. L.,"A Stochastic Analysis of a Modified Gain Extended Kalman Filter with Application to Bearings only Measurements," IEEE Transactions on Automatic Control, Vol. AC-30, no.10, Oct. 1985, pp. 940-949.

[45] Thienel, J. K., Harman, R. R., Bar-Itzhack, I. Y., and Lambertson, M., "Results of the Magnetometer Navigation (MAGNAV) Inflight Experiment," AIAA/AAS Astrodynamics Specialist Conference and Exhibit, August 16-19, Providence, RI, 2004.

[46] Tournes, C., Shtessel, Y., and Shkolnikov, I., "Autopilot for Missiles Steered by Aerodynamic Lift and Divert Thrusters using Nonlinear Dynamic Sliding Manifolds," *Proceedings of the Conference on Guidance, Navigation and Control*, paper AIAA-2005-6382, 2005.

[47] Utkin, V., Guldner, J., and Shi, J., *Sliding Modes in Electromechanical Systems*, Taylor and Francis, London, 1999

[48] Vallado, David A., *Fundamentals of Astrodynamics and Applications*, 2nd ed., Microcosm Press, El Segundo, CA, 2001.

[49] Wise, K.A. and Roy, D.J., "Agile Missile Dynamics and Control," *Journal of Guidance, Control, and Dynamics*, Vol. 21. No. 3, May-June, 1998.

[50] Xin, C. F. and Yueh, W.R., "Optimal Controller for Bank-to-Turn Missile," *Proceedings of IEEE Conference on Decision and Control*, Las Vegas, NV, December,1984.

[51] Xin, M., "A New Method for Suboptimal Control of A Class of Nonlinear Systems," Ph.D Dissertation, University of Missouri-Rolla, December, 2002.

[52] Xin, M. and Balakrishnan,S. N. ,"A New Filtering Technique for a Class of Nonlinear Systems'" CDC02-REG0931, IEEE Conference on Decision and Control, Las Vegas, NV, Dec. 2002.

[53] Xin, M. and Balakrishnan, S. N., "A New Method for Suboptimal Control of a Class of Nonlinear Systems," *Journal of Optimal Control Applications and Methods*, Vol. 26, 2005, pp. 55-83.

[54] Xin, M. and Balakrishnan, S.N., "Missile Longitudinal Autopilot Design Using a New Suboptimal Nonlinear Control Method," *IEEE Proceedings on Control Theory Applications*, Vol. 150, No. 6, 2003, pp. 577- 584.

[55] Xin, M., Balakrishnan, S.N., and Ohlmeyer, E. ,"Integrated Guidance and Control of Missiles with Theta-D Method," 2004 IFAC Symposium on Aerospace, St. Petersburg, Russia.

[56] Xin, M. and Balakrishnan, S.N., Stansbery, D.T. and Ohlmeyer, E.J., "Nonlinear Missile Autopilot Design with Theta-D Technique," *Journal of Guidance, Control and Dynamics*, May-June, 2004.

[57] Yanushevsky, R. and Boord, W., "New Approach to Guidance Law Design," *Journal of Guidance, Control, and Dynamics*, No. 1, 2005.

[58] Zarchan P., "Tactical and Strategic Missile Guidance", vol. 176, *Progress in Astronautics and Aeronautics,* AIAA Publications, 1998.

VITA

Michael William Dancer was born in Poplar Bluff, MO on November 18, 1981 to Mark and Debi Dancer. He graduated from Poplar Bluff Senior High School in May of 2000 and enrolled at the Missouri University of Science and Technology (then the University of Missouri – Rolla) in the following fall. He received a Bachelor of Science degree in Aerospace Engineering in the spring of 2004 and a Master of Science degree in Aerospace Engineering in May of 2010.

During his time at Missouri S&T, Michael was a member of the Concrete Canoe team for three years and was an original team member of the Miners in Space team, which allowed him to fly aboard NASA's microgravity research plane, known colorfully as the Vomit Comet, in the summer of 2003. Michael has been an active member of the Missouri S&T Satellite Team since the fall of 2003. He is currently the team's Chief Engineer.

Michael has received the Academy of Mechanical and Aerospace Engineer's Student Excellence Award twice for his work on the Miners in Space and M-SAT teams. He, along with coauthor Jason Searcy, received 1st place in the 2007 Frank J. Redd Student Paper Competition, earning a $10,000 prize. The competition is held annually at the Small Satellite Conference in Logan, UT.